AD-A193 493 THE ELECTROCHEMICAL BEHAVIOR OF DISPERSIONS OF SPHERICAL ULTRAMICROELECTRODES(U) UTAH UNIV SALT LAKE CITY DEPT OF CHEMISTRY S PONS ET AL. 30 JUL 86 TR-61 1/1

UNCLASSIFIED N00014-83-K-0470 F/G 7/4 NL

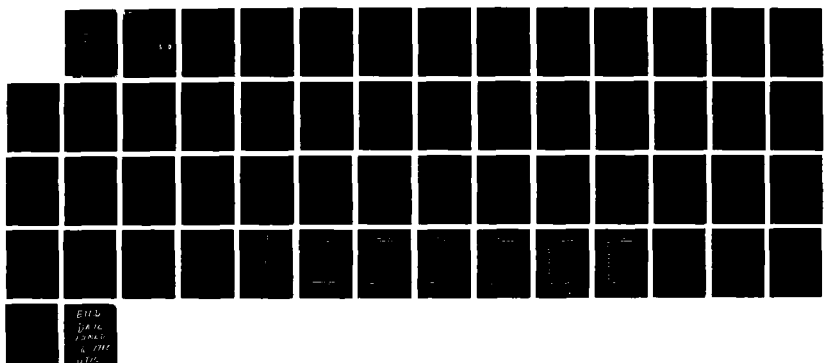

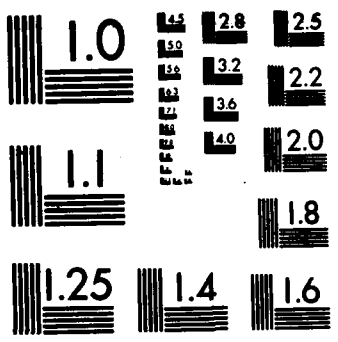

(4)

OFFICE OF NAVAL RESEARCH

Contract N00014-83-K-0470-P00003

Task No. NR 359-718

TECHNICAL REPORT # 61

The Electrochemical Behavior of Dispersions of Spherical Ultramicroelectrodes

By

Stanley Pons, D. Rolison, J. Ghoroghchian, M. Fleischmann

Prepared for Publication in

Journal of Physical Chemistry

University of Utah
Department of Chemistry
Salt Lake City, Utah 84112

July 30, 1986

SECURITY CLASSIFICATION OF THIS PAGE (When Data Entered)

REPORT DOCUMENTATION PAGE		READ INSTRUCTIONS BEFORE COMPLETING FORM
1. REPORT NUMBER: 61	2. GOVT ACCESSION NO.	3. RECIPIENT'S CATALOG NUMBER
4. TITLE (and Subtitle): The Electrochemical Behavior of Dispersions of Spherical Ultramicroelectrodes		5. TYPE OF REPORT & PERIOD COVERED: Technical Report # 61
		6. PERFORMING ORG. REPORT NUMBER
7. AUTHOR(s): Stanley Pons, D. Rolison, J. Ghoroghchian, M. Fleischmann		8. CONTRACT OR GRANT NUMBER(s): N00014-83-K-0470-P0003
9. PERFORMING ORGANIZATION NAME AND ADDRESS: University of Utah, Department of Chemistry, Salt Lake City, UT 84112		10. PROGRAM ELEMENT, PROJECT, TASK AREA & WORK UNIT NUMBERS: Task No. NR 359-718
11. CONTROLLING OFFICE NAME AND ADDRESS: Office of Naval Research, Chemistry Program - Chemistry Code 472, Arlington, Virginia 22217		12. REPORT DATE: July 30, 1986
		13. NUMBER OF PAGES
14. MONITORING AGENCY NAME & ADDRESS (if different from Controlling Office)		15. SECURITY CLASS. (of this report): Unclassified
		15a. DECLASSIFICATION/DOWNGRADING SCHEDULE

16. DISTRIBUTION STATEMENT (of this Report)

This document has been approved for public release and sale; its distribution unlimited.

17. DISTRIBUTION STATEMENT (of the abstract entered in Block 20, if different from Report)

18. SUPPLEMENTARY NOTES

19. KEY WORDS (Continue on reverse side if necessary and identify by block number)

Ultramicroelectrodes, Dispersions

20. ABSTRACT (Continue on reverse side if necessary and identify by block number)

It is shown that it is possible to carry out electrochemical reactions in poorly conducting and non-conducting media by means of bipolar electrolyses with dispersions.

Keywords

DD FORM 1 JAN 73 1473 EDITION OF 1 NOV 65 IS OBSOLETE

S/N 0102-LF-014-6601

Unclassified

SECURITY CLASSIFICATION OF THIS PAGE (When Data Entered)

Rev May 15 '86

J. Phys. Chem.

THE ELECTROCHEMICAL BEHAVIOR OF DISPERSIONS OF SPHERICAL ULTRAMICROELECTRODES

Martin Fleischmann***, Jamal Ghoroghchian*,
Debra Rolison**, and Stanley Pons*[1]

*Department of Chemistry, University of Utah
Salt Lake City, Utah 84112, U.S.A.

**Surface Chemistry Branch, Naval Research Laboratory,
Washington, D.C. 20375-5000, U.S.A.

***Department of Chemistry, University of Southampton
Southampton, Hants, SO9 5NH ENGLAND

[1] To whom correspondence should be addressed.

ABSTRACT

It is shown that it is possible to carry out electrochemical reactions in poorly conducting and non-conducting media by means of bipolar electrolyses with dispersions. Polarization equations are predicted for highly simplified models based on the concept of the mixture potential, the surface reactions being assumed to be rate determining. Results for hydrogen evolution/oxidation and oxygen evolution/reduction show that the interpretation of polarization curves at high field strengths will have to take into account the effects of diffusion. The results also show that it should be possible to investigate, monitor and modify heterogeneous catalyses of reactions in the liquid phase by means of the Faradaic currents induced by the electric fields.

INTRODUCTION

The construction and behavior of microdisk (see e.g. (1-19)) microring (19,20) and microsphere (see e.g. (19,21-23)) electrodes have been discussed extensively. The high rates of stationary mass transfer in the developing quasi-spherical diffusion fields allow the measurement of the kinetics of fast electrode reactions (5,13,19,21,22) and of fast reactions in solution coupled to electrode reactions (14,15) under steady state conditions. The spherical potential field decreases charging times so that fast transient techniques can be readily applied (13); the low Ohmic losses in solution have also allowed measurements to be made in solutions containing only low (or effectively zero) concentrations of support electrolyte as well as in glasses at low temperatures (17,24) and even in the vapor phase (25).

The modest scale-up of reactions at microelectrodes requires the use of special structures such as of embedded reticulated foams (26) or fibers (27). Exploitation of the special advantages of microelectrodes for synthesis (e.g. the ease of work-up and the extension of the solvent range in the absence of support electrolyte (18)) however requires the use of three-dimensional electrodes. Bipolar electrolyses on dispersions of spherical particles have been proposed and the behavior of such electrodes in the presence of a single redox couple has been analyzed for a number of limiting conditions (28); these systems represent an extension of the concepts used in bipolar fluidized bed electrodes (29) to the area of microelectrodes. In this paper we extend the analysis to the behavior of the dispersions in the presence of two reversible or two irreversible electrode reactions

using the simplest model, Figure 1A (28) and compare this behavior to that observed at the mixture potentials in systems containing relatively high concentrations of electrolyte (30,31); colloidal systems at the relevant mixture potentials have been extensively investigated in recent years in the context of the catalysis of the photodecomposition of water (e.g. see (32-41)). It should be noted that the size range of the particles which will be most frequently used in dispersion electrolyses (10^{-5}cm < a < 10^{-3}cm) is intermediate to that of the colloidal systems (typically 10^{-6}cm) and fluidized bed electrodes (typically 10^{-2}cm).

The behavior in the presence of two redox systems is compared to that observed for a single redox reaction and to experimental data for two electrode reactions on Pt-dispersions: hydrogen evolution/oxidation in conductivity water and oxygen evolution/reduction in dilute potassium hydroxide solutions. The behavior of other systems and applications to synthesis (42) and the use of supported metal catalyst particles (43) will be discussed elsewhere.

Mathematical description of dispersion electrolysis control by a single redox couple.

Dispersion electrolyses will usually be carried out using low or zero concentrations of support electrolyte. For the generation of a cation from an uncharged substrate

$$O^+ + e \rightleftharpoons R \qquad [A]$$

or the converse case of the generation of an anion

$$O + e \rightleftharpoons R^- \qquad [B]$$

the charge density generated in the reactions will be compensated by counterions either from deliberately added low concentrations of support electrolyte or from impurities or ions generated by autoionization of the solvent. For the likely range of particle radii, a, 10^{-5}cm < a < 10^{-3}cm, the steady state mass transfer coefficient, k_m,

$$k_m \simeq \frac{D}{a} \qquad [1]$$

is so high that the surface reaction is likely to be rate controlling at low and intermediate overpotentials for the majority of reactions. In the simplest possible model we assume (28) that the reactions on the anodic and cathodic parts of a representative spherical particle do not significantly perturb the equipotentials (i.e. the surface of a particle experiences the mean field). The overpotential $\eta(V)$ at the position (a,θ) is then given by

$$\eta = -\Delta\phi_s = -\frac{V_{appl}\, a}{L}\left(\cos\theta + \cos\lambda\right) \qquad [2]$$

where V_{appl} (V) is the applied voltage, L(cm) is the distance between

the feeder electrodes and λ defines the position at which $\eta=0$ (see Figure 1A for the coordinate system). For a reaction following the simple polarization equation

$$i = i_o\left[\exp\left(\frac{-\alpha\eta F}{RT}\right) - \exp\left(\frac{(1-\alpha)\eta F}{RT}\right)\right] \qquad [3]$$

we obtain the total current into a single particle

$$I = 2\pi a^2 \int_0^{\pi-\lambda} i \sin\theta \, d\theta$$

$$= \frac{2\pi i_o RTLa}{FV_{applied}\alpha(\alpha-1)}\left[(\alpha-1)\exp(\alpha\gamma\cos\lambda)\exp(\alpha\gamma)\right. \qquad [4]$$

$$\left. - \alpha\exp((\alpha-1)\gamma\cos\lambda)\exp((\alpha-1)\gamma) + 1\right]$$

where $$\gamma = \frac{FV_{applied}\, a}{RTL} \qquad [5]$$

and the division between the net cathodic and anodic areas is defined by

$$\exp(\gamma\cos\lambda) = \left(\frac{\alpha}{\alpha-1}\right)\frac{\sinh((\alpha-1)\gamma)}{\sinh(\alpha\gamma)} \qquad [6]$$

In the dispersion each bipolar particle presents a shunt resistance to the overall solution resistance and we obtain the overall polarization curve

$$I_T = \frac{V_{appl}}{\rho_s L} + \frac{4\pi i_o RTLNa^2}{FV_{appl}\alpha(\alpha-1)}\left[(\alpha-1)\exp(\alpha\gamma\cos\lambda)\exp(\alpha\gamma)\right.$$

$$\left. -\alpha\exp((\alpha-1)\gamma\cos\lambda)\exp((\alpha-1)\gamma) + 1\right] \qquad [7]$$

where I_T (Amps cm^{-2}) is the cross-sectional current density through the dispersion, N is the number of particles per unit volume and ρ_s (Ohm cm) is the solution resistivity. The non-Faradaic by-pass current $V_{appl}/\rho_s L$ can be determined from the background current in the absence of the dispersion. We can therefore cast [7] in the dimensionless form

$$\frac{I_p \gamma}{3 i_o V} = \left(I_T - \frac{V_{appl}}{\rho_s L} \right) \frac{\gamma}{3 i_o V} \qquad [8]$$

$$= \frac{1}{\alpha(\alpha-1)} \left[(\alpha-1) \exp(\alpha\gamma\cos\lambda) \exp(\alpha\gamma) - \alpha \exp((\alpha-1)\gamma\cos\lambda) \exp((\alpha-1)\gamma) + 1 \right]$$

where I_p (Amps cm^{-2}) is the cross-sectional Faradaic current density through the particles and v (cm^3 cm^{-3}) is the volume of the particles of the dispersion added per unit cell volume. Equation [8] compares dispersion electrolysis most directly with the conventional form, [3], of the polarization equation. Direct comparisons of experimental data with the predicted forms of the polarization equations may be carried out by writing [8] (and subsequent equations) as

$$\frac{I_p}{3 i_c V} = \frac{1}{\alpha(\alpha-1)\gamma} \left[(\alpha-1) \exp(\alpha\gamma\cos\lambda) \exp(\alpha\gamma) - \alpha \exp((\alpha-1)\gamma\cos\lambda) \exp((\alpha-1)\gamma) + 1 \right] \qquad [9]$$

For the special case $\alpha=0.5$, $\lambda = \pi/2$ we obtain

$$\frac{I_p}{3 i_c V} = \frac{4}{\gamma} \left[\cosh\left(\frac{\gamma}{2}\right) - 1 \right] \qquad [10]$$

while the special case $\alpha=1$ gives

$$\exp(\gamma\cos\lambda) = \frac{\gamma}{\sinh\gamma} \qquad [11]$$

and [12]

$$\frac{I_p}{3i_0V} = \frac{\exp\gamma}{\sinh\gamma} - \left(\frac{1+\gamma}{\gamma}\right) - \frac{1}{\gamma}\ln\left(\frac{\gamma}{\sinh\gamma}\right)$$

It should be noted that in view of the bipolarity of the particles the polarization curve for a given value of α is identical to that for $(1-\alpha)$. In consequence, the dependence of the polarization curves on α is diminished compared to that observed for planar electrodes, Figure 2A.

The effect of particle rotation.

The formation and removal of surface layers (e.g. Pt-H or Pt-O) due to particle rotation will contribute further Faradaic components to the current. The rotational frequency will be (28)

$$\nu = \frac{\omega}{2\pi} = \left(\frac{15RT}{32\pi^3 \mathbf{N} a^5 \rho}\right)^{\frac{1}{2}} \qquad [13]$$

where **N** (number mol^{-1}) is Avogadro's number and ρ (g cm^{-3}) is the density. The frequency will lie in the range 10^{-2} - 10^{4} revolutions s^{-1} for the likely range of particle radii. If a monolayer charge $nF\Omega$ is continuously formed and stripped by the particle rotation, then at

such a limiting condition the current flow will be

$$I_R \simeq 4\pi a^2 n F \Omega \nu \qquad [14]$$

where Ω (moles cm^{-2}) is the saturation monolayer coverage and n charges are transferred for each adsorbed species. The current flow in a slice of thickness 2a will be

$$2aNI_R = 8\pi a^3 n F \Omega \nu N \qquad [15]$$

This current can be compared to I_p by taking

$$\frac{2aNI_R}{3i_oV} = \frac{2nF\Omega\nu}{i_o} \qquad [16]$$

Effects of changes in the polarization equation.

Simple changes in the polarization equation such as the replacement of [3] by

$$i = i_o\left[\exp\left(\frac{-\alpha n \eta F}{RT}\right) - \exp\left(\frac{(1-\alpha) n \eta F}{RT}\right)\right] \qquad [17]$$

lead to equations of the form

$$\frac{I_p}{3i_0v} = \frac{1}{\alpha(\alpha-1)\gamma}\left[(\alpha-1)\exp(\alpha n\gamma\cos\lambda)\exp(\alpha n\gamma)\right. \qquad [18]$$
$$\left. -\alpha\exp((\alpha-1)n\gamma\cos\lambda)\exp((\alpha-1)n\gamma)+1\right]$$

with λ being defined by

$$\exp(n\gamma\cos\lambda) = \left(\frac{\alpha}{\alpha-1}\right)\frac{\sinh((\alpha-1)n\gamma)}{\sinh(\alpha n\gamma)} \qquad [19]$$

It follows that if the parameter $n\gamma$ is replaced by a parameter Ψ, then the shapes of the derived polarization curves will be the same as those for a 1-electron transfer reaction; if the currents are plotted against γ, then the shapes of the predicted curves will be changed. However, in practice the effects on the polarization equation of a sequence of reaction steps will usually be more complicated than is indicated by simple changes such as from equation [3] to [17].

Control by two redox reactions.

We discuss this case as the simplest possible example of a catalytic reaction and assume that homogeneous electron transfer is slow compared to the rates of the electrode reactions (compare (31)). We develop the analysis by analogy to the concept of mixture potentials (44) which has been extensively applied to a range of electrochemical

problems (45). In the absence of any externally applied electric field the particles will adopt a potential such that the net anodic current density of the couple having the more negative reversible potential is equal to the net cathodic current density of the couple with the more positive reversible potential[1]

$$i_{o1}\left[\exp\left(\frac{(1-\alpha_1)\eta_1^m F}{RT}\right) - \exp\left(\frac{-\alpha_1\eta_1^m F}{RT}\right)\right] = i_{o2}\left[\exp\left(\frac{-\alpha_2\eta_2^m F}{RT}\right) - \exp\left(\frac{(1-\alpha_2)\eta_2^m F}{RT}\right)\right] \quad [20]$$

where η_1^m - η_2^m are the overpotentials at the mixture potentials. Equation [20] can be solved with

$$\eta_2^m - \eta_1^m = -\left(E_{2,r} - E_{1,r}\right) = \Delta E \quad [21]$$

---

[1] In this simple model we assume that there is no interaction between the two reactions as would be caused, for example, by competitive adsorption of reactants, intermediates or products of the two component reactions or the reaction of adsorbed reactants or intermediates of the two redox couples.

to give the mixture potential; ΔE will be a negative quantity. The rate of the two redox reactions can then be derived from [20].

It has been shown that a large number of paired redox reactions in conventional electrolyte solutions are catalyzed by noble metals which adopt this mixture potential (46). An extensive series of investigations has shown that the reactions may be controlled by slow electrode reactions (see e.g. (47,31)) or else by diffusion with a Nernst equilibrium at the surface (see e.g.(30,48,49)); see also references cited in (30,31,47-49).

An exact and general analysis of the problem in the presence of an externally applied electric field requires the solution of the differential equations governing diffusion and migration to the particles, the reactions on the surface being boundary conditions for these solutions (28). To simplify the analyses we will assume here that i_{O_1} and i_{O_2} are sufficiently small so that the potential of the surface follows the applied external field, Figure 1A, and so that the effects of mass transfer can be neglected. We now define η_1^m and η_2^m as being the overpotentials at which there is no local net Faradaic current so that we can write

$$\eta_1 = \eta_1^m - \frac{V_{appl}\, a}{L}\left(\cos\theta + \cos\lambda\right) \qquad [22]$$

$$\eta_2 = \eta_2^m - \frac{V_{appl}\, a}{L}(\cos\theta + \cos\lambda) \qquad [23]$$

$$= \eta_1^m + \Delta E - \frac{V_{appl}\, a}{L}(\cos\theta + \cos\lambda)$$

The total external cathodic (or anodic) current is obtained by taking into account the contributions from both redox couples (see Figure 1B for the general case ($2 V_{appl}\, a)/L > \Delta E$)

$$I_c = -2\pi a^2 \int_0^{\pi-\lambda} i_1 \sin\theta\, d\theta + 2\pi a^2 \int_0^{\pi-\lambda} i_2 \sin\theta\, d\theta \qquad [24]$$

With some rearrangement we obtain

$$I_c = \frac{2\pi a^2 i_{c1}}{\gamma\alpha_1(\alpha_1-1)}\left[(\alpha_1-1)\exp\left(\frac{-\alpha_1\eta_1^m F}{RT}\right)\exp(\alpha_1\gamma\cos\lambda)\exp(\alpha_1\gamma)\right.$$

$$-\alpha_1\exp\left(\frac{(1-\alpha_1)\eta_1^m F}{RT}\right)\exp((\alpha_1-1)\gamma\cos\lambda)\exp((\alpha_1-1)\gamma)$$

$$\left.-(\alpha_1-1)\exp\left(\frac{-\alpha_1\eta_1^m F}{RT}\right)+\alpha_1\exp\left(\frac{(1-\alpha_1)\eta_1^m F}{RT}\right)\right]$$

$$+\frac{2\pi a^2 i_0}{\gamma\alpha_2(\alpha_2-1)}\left[(\alpha_2-1)\exp\left(\frac{-\alpha_2(\Delta E+\eta_1^m)F}{RT}\right)\exp(\alpha_2\gamma\cos\lambda)\exp(\alpha_2\gamma\right.$$

[25]

$$-\alpha_2 \exp\left(\frac{(1-\alpha_2)(\Delta E+\eta_1^m)F}{RT}\right) \exp\left((\alpha_2-1)\gamma\cos\lambda\right) \exp\left((\alpha_2-1)\gamma\right)$$

$$-(\alpha_2-1)\exp\left(\frac{-\alpha_2(\Delta E+\eta_1^m)F}{RT}\right)+\alpha_2\exp\left(\frac{(1-\alpha_2)(\Delta E+\eta_1^m)F}{RT}\right)\Bigg]$$

The angle λ is defined by the equality of the total net cathodic and anodic currents:

$$-\int_0^{\pi-\lambda} i_1 \sin\theta\, d\theta + \int_0^{\pi-\lambda} i_2 \sin\theta\, d\theta$$

$$= \int_{\pi-\lambda}^{\pi} i_1 \sin\theta\, d\theta - \int_{\pi-\lambda}^{\pi} i_2 \sin\theta\, d\theta \qquad [26]$$

i.e. $$\int_0^{\pi} i_1 \sin\theta\, d\theta = \int_0^{\pi} i_2 \sin\theta\, d\theta \qquad [27]$$

giving

$$\frac{i_{o1}}{\alpha_1(\alpha_1-1)}\left[(\alpha_1-1)\exp\left(-\frac{\alpha_1\eta_1^m F}{RT}\right)\exp(\alpha_1\gamma\cos\lambda)\sinh(\alpha_1\gamma)\right. \quad [28]$$

$$\left. -\alpha_1\exp\left(\frac{(1-\alpha_1)\eta_1^m F}{RT}\right)\exp((\alpha_1-1)\gamma\cos\lambda)\sinh((\alpha_1-1)\gamma)\right]$$

$$= \frac{i_{o2}}{\alpha_2(\alpha_2-1)}\left[\alpha_2\exp\left(\frac{(1-\alpha_2)(\Delta E+\eta_1^m)F}{RT}\right)\exp((\alpha_2-1)\gamma\cos\lambda)\sinh((\alpha_2-1)\right.$$

$$\left. -(\alpha_2-1)\exp\left(-\frac{\alpha_2(\Delta E+\eta_1^m)F}{RT}\right)\exp(\alpha_2\gamma\cos\lambda)\sinh(\alpha_2\gamma)\right]$$

Equation [28] can be solved with [20] and [21] to give λ as a function of the experimental conditions and the polarization curve can then be derived from [25].

It has been shown above that the polarization curves for a single redox couple do not depend markedly on α in the middle range of this parameter. We therefore restrict attention here to the special case $\alpha_1 = \alpha_2 = 0.5$, $i_{o1} = i_{o2}$ giving

$$\lambda = \frac{\pi}{2} \quad \text{for all } \gamma \qquad [29]$$

and

$$\frac{I_p}{3i_c V} = \frac{4}{\gamma}\left[\cosh\left(\frac{\Delta EF}{4RT}+\frac{\gamma}{2}\right)\right.$$

$$\left.+\cosh\left(\frac{\Delta EF}{4RT}-\frac{\gamma}{2}\right)-2\cosh\left(\frac{\Delta EF}{4RT}\right)\right] \qquad [30]$$

We are also interested in the total net current for each redox couple e.g.

$$I_1 = 2\pi a^2\int_0^{\pi} i_1 \sin\theta\, d\theta$$

$$= \frac{4\pi a^2 i_{01}}{\gamma\alpha_1(\alpha_1-1)}\left[(\alpha_1-1)\exp\left(\frac{-\alpha_1\eta_1^m F}{RT}\right)\exp(\alpha_1\gamma\cos\lambda)\sinh(\alpha_1\gamma)\right. \qquad [31]$$

$$\left.-\alpha_1\exp\left(\frac{(1-\alpha_1)\eta_1^m F}{RT}\right)\exp((\alpha_1-1)\gamma\cos\lambda)\sinh((\alpha_1-1)\gamma)\right]$$

For the special case $\alpha_1 = \alpha_2 = 0.5$, $i_{01} = i_{02}$ we obtain

$$\frac{I_N}{3i_oV} = \frac{8}{\gamma} \sinh\left(\frac{\Delta EF}{4RT}\right) \sinh\left(\frac{\gamma}{2}\right) \qquad [32]$$

where I_N (Amps cm^{-2}) is the net cross-sectional current density for each of the redox couples.

$I_p/(3i_ov)$ is plotted against γ in Figure 2B (equation [30]). It can be seen that I_p increases rapidly with $\Delta EF/4RT$; this increase is so marked that it is unlikely that the simple model illustrated in Figure 1B will be adequate for large values of ΔE. The shapes of the polarization curves however are nearly independent of $\Delta EF/4RT$ so that it is only possible to distinguish the case of control by two redox processes from that by one redox reaction, Figure 2A, by virtue of the observation of an anomalously low value of i_o.

The plots of $I_N/3i_ov$ against γ, Figure 2C, show that it is possible to increase the net rate of each redox process by applying an electric field to the particles and this could prove to be useful in certain examples of catalysis. It can be seen that the ratios I_N/I_P approach a limit with increasing values of $\Delta EF/4RT$ even for low values of γ: the ratios are already independent of ΔE for ΔE as low as ~0.25V. Since I_P is measured experimentally it follows that the form of the $I_N - \gamma$ relationship can be derived indirectly. It should therefore be possible to investigate and monitor catalytic reactions involving redox processes by measuring the polarization curves for the dispersed catalyst particles. It should be noted that such measurements can

be made in solvents having effectively zero ionic conductivity (see further below) and, equally, on dispersions made of materials showing low electronic conductivity (e.g. semiconductors) (43).

Control by two irreversible reactions.

For sufficiently slow redox reactions or, more usually, in the case of the intervention of chemical reactions leading to the formation of electroinactive species, one or both of the component reactions must be regarded as being irreversible. There will be many special cases; here we restrict attention to two of these:

A) The cathodic reaction of redox couple 1 is balanced by the anodic reaction of redox couple 2

B) The anodic reaction of redox couple 1 is balanced by the cathodic reaction of redox couple 2.

The special case A.

At the mixture potential we have

$$i_{o1} \exp\left(\frac{-\alpha \eta_1^m F}{RT}\right) = i_{o2} \exp\left(\frac{(1-\alpha_2)\eta_2^m F}{RT}\right) \qquad [33]$$

which can be solved together with [21]. In the presence of an applied field, the overpotentials are given by [22] and [23] and the total cathodic and anodic currents on each particle are obtained by integrating over the range 0-π. We obtain

$$I_c = \frac{4\pi a^2 i_{o1}}{\alpha_1 \gamma} \exp\left(\frac{-\alpha_1 \eta_1^m F}{RT}\right) \exp\left(\alpha_1 \gamma \cos\lambda\right) \sinh\left(\alpha_1 \gamma\right) \quad [34]$$

and determine λ from [21] with

$$\frac{i_{o1}}{\alpha_1} \exp\left(\frac{-\alpha_1 \eta_1^m F}{RT}\right) \exp\left(\alpha_1 \gamma \cos\lambda\right) \sinh\left(\alpha_1 \gamma\right)$$

$$= \frac{i_{o2}}{(1-\alpha_2)} \exp\left(\frac{(1-\alpha_2)(\eta_1^m + \Delta E)F}{RT}\right) \exp\left((\alpha_2 - 1)\gamma \cos\lambda\right) \sinh\left((1-\alpha_2)\gamma\right) \quad [35]$$

The special case $\alpha_1 = \alpha_2 = 0.5$, $i_{o1} = i_{o2}$ gives $\lambda = \pi/2$

and $$\frac{I_p}{3 i_o V} = \frac{2}{\gamma} \exp\left(\frac{\Delta E F}{4RT}\right) \sinh\left(\frac{\gamma}{2}\right) \quad [36]$$

<u>The special case B.</u>

At the mixture potential we have

$$i_{o1} \exp\left(\frac{(1-\alpha_1)\eta_1^m F}{RT}\right) = i_{o2} \exp\left(\frac{-\alpha_2 \eta_2^m F}{RT}\right) \quad [37]$$

which is solved in conjunction with [21]. In this case we obtain

$$I_c = \frac{4\pi a^2 i_{o1}}{(1-\alpha_1)\gamma} \exp\left(\frac{(1-\alpha_1)\eta_1^m F}{RT}\right) \exp\left((\alpha_1-1)\gamma\cos\lambda\right) \sinh\left((1-\alpha_1)\gamma\right) \qquad [38]$$

with λ being determined from [21] with

$$\frac{i_{o1}}{(1-\alpha_1)} \exp\left(\frac{(1-\alpha_1)\eta_1^m F}{RT}\right) \exp\left((\alpha_1-1)\gamma\cos\lambda\right) \sinh\left((1-\alpha_1)\gamma\right) \qquad [39]$$

$$= \frac{i_{o2}}{\alpha_2} \exp\left(\frac{-\alpha_2(\eta_1^m + \Delta E)F}{RT}\right) \exp(\alpha_2\gamma\cos\lambda) \sinh(\alpha_2\gamma)$$

The special case $\alpha_1 = \alpha_2 = 0.5$, $i_{o1} = i_{o2}$ gives $\lambda = \pi/2$

and $$\frac{I_p}{3i_o V} = \frac{2}{\gamma} \exp\left(\frac{-\Delta E F}{4RT}\right) \sinh\left(\frac{\gamma}{2}\right) \qquad [40]$$

Comparison of [36] with [40] shows that the rates are much higher for case B than for case A.

EXPERIMENTAL

Two suitable cell designs which have been used in the present investigation are illustrated in Figures 3A and B. The first had concentric platinum foil feeder electrodes with a 0.5cm interelectrode

gap. The microparticles were kept in suspension by sparging gas through the fine sintered disk at the base of the cell. The cell was used for measurements of the evolution/oxidation of hydrogen; hydrogen-nitrogen gas mixtures of the appropriate composition were therefore sparged into the solution the total gas pressure in the cell being kept at one atmosphere.

The second cell, Figure 3B, had a plane parallel capillary gap configuration with an interelectrode gap of 0.5mm. The feeder electrodes were again made of platinum foil (0.5μm). Particles were kept in suspension in a small reservoir by bubbling gas and the dispersion was pumped through the flow circuit using a Monostate Ministaltic pump. Typical flow rates were 15cm s^{-1} and were measured by a Gilmont Instruments flow meter. Controlled voltages were applied to the cells using a Kepco regulated power supply model HB-6M. Current-potential curves were recorded point-by-point, a HI-TEK digital integrator/DVM being used to smooth out current fluctuations.

Prior to each experiment the background current due to the solvent (water) or electrolyte (potassium hydroxide solution) in the absence of the dispersion was measured. An appropriate amount of platinum powder (Johnson-Matthey) was then added to give a particle concentration in the range 10^8 - 10^9 cm^{-3} (based on the tap density quoted by the manufacturer). The required amount was of the order 3mg Pt cm^{-3}; the average particle diameter was 2.5 micrometers; the geometry was assumed to be spherical. The polarization curves were then redetermined for the chosen conditions.

Conductivity water was prepared by triple distillation in a glass

still from "in-house" distilled water. The first stage contained 0.1mM potassium permanganate and potassium hydroxide to raise the pH to ~8.0; the second stage contained phosphoric acid. Potassium hydroxide solutions were made up using J.T. Baker Chemical Company KOH. Hydrogen and nitrogen, or the gas mixtures used were UHP grade from IGP and were used as supplied. Glassware was cleaned using a mixture of HNO_3/H_2SO_4 and was then rinsed thoroughly using triply distilled water.

RESULTS AND DISCUSSION

Hydrogen evolution/oxidation

Figure 4 illustrates the polarization curves obtained for hydrogen evolution/oxidation in conductivity water at low values of the applied field. The background current in the absence of the platinum particles shows that the water maintained a specific resistivity in excess of 10^7 Ohm cm in the cells and circulation systems used in these experiments. Electrolyte impurities therefore remained at very low levels (the specific resistivity of pure water has been given as 1.69×10^7 Ohm cm (50) and the theoretical limit is 1.82×10^7 Ohm cm). Addition of the platinum particles gave the expected increase in the Faradaic current; this current was found to be proportional to the amount of particles added (expressed here as the volume of the dispersed phase per unit volume of liquid) and to the partial pressure of hydrogen sparged into the cell, Figure 4.

Figures 5A and B show that at low applied fields the experimental data fit closely to the special case (10) (for $\alpha = 0.5$) of the predicted equation [8] based on the simple polarization equations [3] or [17]

(with n=2). The data do not permit a clear distinction to be made between the kinetic forms although it appears that [17] is to be preferred as [3] consistently gave plots lying above the maximum permitted rate at higher values of the applied field. The simple first order dependence of the polarization curves on the partial pressure of hydrogen as well as the fit of the curves to equation [10] shows that the behavior of the bipolar system is controlled by a single overall hydrogen evolution/oxidation reaction such as [A] or [B]

$$2H^+ + 2e \rightleftharpoons H_2 \qquad [A]$$

$$2H_2O + 2e \rightleftharpoons H_2 + 2OH^- \qquad [B]$$

Control of hydrogen evolution by [B] and oxidation by [A] would require a fit of the experimental data to [30] or to the special case [A], equation [36].

In Figures 5A and B the experimental data have been fitted to the predicted plots using the apparent exchange current density, i_o, as the adjustable parameter. The required i_o is high even allowing for the large real surface area of the particles (the ratio of the real to the apparent area lay in the range 5-10). This large exchange current density shows that the particles maintained a very high level of catalytic activity and that as in other investigations of the hydrogen evolution/ionization reaction we must assume that the surface reaction is close to reversibility since i_o approaches the value predicted from the mass transfer coefficient, equation [1]. The behavior of

dispersion electrodes under conditions which include the effects of diffusion (28) will be discussed further elsewhere (51). It should be noted that in view of the high rate of the reaction the data show no evidence for the deposition/removal of adsorbed hydrogen, the expected value of equation [16] being 10^{-2} - 10^{-1} at $\gamma \approx 1$ with the same value of i_o as that used in fitting the experimental data to the predicted equations and a value $\Omega \approx 10^{-7}$ moles cm^{-2} allowing for the high real area of the particles (see also section on oxygen evolution/reduction.

At higher values of the applied field Figures 5C and D indicate at first sight that behavior according to the kinetic law [3] is to be preferred to that according to [17] but the fit obtained in Figure 5C must be regarded as being fortuitous. At these high rates the reaction on the particles will be diffusion limited by the anodic process as is indicated by Figure 5D. Indeed the continued fit to [10] implied by Figure 5C would require a kinetically controlled current density in excess of 500mA cm^{-2} on the apparent surface area of the particles if the current within each layer of thickness $\approx 2a$ is regarded as becoming wholly Faradaic i.e. if each layer is effectively screened by the adjacent layers of the dispersion. Figure 5D requires that the diffusion limited current should reach this value using the same assumption of the screening of adjacent layers of the dispersion. However, the diffusion limited current will be maximally

$$i_{lim} = 2 \times 3 \cdot 22 \frac{FD}{a} (C_{H_2})_{bulk} \simeq 50 mA\, cm^{-2} \qquad [41]$$

the factor 3.22 being due to generation of hydrogen on the cathodic areas adjacent to the anodic areas of the bipolar particles (28). The discrepancy between the two values points to the particles being effectively screened at a distance 5-6a at the limiting current density rather than at the value 2a which was assumed previously (28). It should be noted that the proportionality of the observed current to the number concentration of added particles does indeed show that the particles are screened from the feeder electrodes by adjacent layers of particles.

Oxygen evolution/reduction

Figure 6 shows that as for the case of hydrogen evolution/oxidation the rate of the bipolar oxygen evolution/reduction is proportional to the amount of the added dispersion for low values of the applied polarization.[2] At higher values of Y the plots diverge: the decrease of $i_pY/3v$ with increasing v shows that the solution is being depleted of oxygen during passage through the cell even though this is being regenerated in the anodic reaction on the bipolar particles. It should be noted that in these experiments the solution was presaturated with oxygen outside the cell in distinction to the experiments with hydrogen where this gas (or the hydrogen-helium gas mixture) was directly sparged into the cell.

The form of the polarization curves, Figure 6, is clearly more complex than for the case of hydrogen evolution/oxidation, Figures 4

[2] In view of the complexity of the phenomena observed in the oxygen system, these are presented as plot of $I_pY/3v$ versus Y rather than as plots of the dimensionless parameter $I_pY/3i_ov$.

and 5. Three separate steps can be distinguished on the plots at low hydroxide concentrations, Figure 7. The magnitude of the first of these can be attributed to the formation and reduction of an oxide layer due to the rotation of the particles, equations [15] and [16], provided Ω in these equations is scaled by the true surface area of the particles and the screening distance ≈2a is replaced by ≈6a. This process can be observed in the case of the oxygen system because of the irreversibility of the oxygen evolution/reduction: for the case of hydrogen evolution/oxidation the corresponding process is masked by the high rate of the main Faradaic reaction. Oxide formation/reduction can also be seen on the plots in Figure 6 which show that the reaction is detected at surprisingly low values of Y (≈2). Oxygen evolution/reduction is also seen at low values of Y, Figures 6 and 7. This early onset of the reactions can probably be attributed to aggregation of the particles in the alkaline media so that each aggregate experiences a higher potential difference than is indicated by the dimension of the individual particles.

The height of the polarization curves increased only slowly with hydroxide concentration in the accessible range 10^{-6} - 10^{-4} M indicating that the behavior of the dispersion electrolysis was controlled by the reduction of oxygen rather than oxygen evolution. Figure 7 shows that two limiting currents could be detected at low hydroxide concentrations in addition to that due to oxide formation/reduction. It is likely that the two waves are due respectively to

$$O_2 + H_2O + 2e \longrightarrow HO_2^- + OH^- \qquad [C]$$

and $$O_2 + 2H_2O + 4e \longrightarrow 4OH^- \qquad [D]$$

together with intervening decomposition of HO_2^-:

$$2HO_2^- \longrightarrow O_2 + 2OH^- \qquad [E]$$

Detailed interpretation of the kinetics must therefore be based on the control of the dispersion electrolysis by two irreversible electrode reactions, at least for the case of the first wave (51).

CONCLUSIONS

The data presented for the hydrogen evolution/oxidation and oxygen evolution/reduction reactions show that it is possible to study electrode processes in poorly conducting or non-conducting media by means of bipolar electrolyses of dispersions. The results obtained for the first system fit predictions derived from a simple model based on the concepts of the mixture potential (44); it is clear, however, that both for this system and for oxygen evolution/reduction the effects of mass transfer (28) must be taken into account.

The conditions used for the experiments reported in this paper are close to those of heterogeneous liquid phase catalyses; it is clear therefore that catalytic processes could be investigated (and monitored) provided electron transfer is involved. Catalytic reactions could also be investigated if no electron transfer is involved provided

one couple undergoes a redox reaction. As measurements can be made in non-conducting media it is evident that such investigations could be extended to semiconductor (and possibly insulator) catalysts. Results for catalysts on oxide and zeolite supports (43) (where the amount iof precious metal per unit volume of solution is greatly reduced) as well as applications to syntheses (42) will be reported elsewhere. Investigations of catalytic systems will require extensions of the modelling which will have to include the effects of reactions and concentration changes in solution. The results obtained also show that it should be possible to accelerate (or modify) catalyses by means of externally applied fields and the consequent Faradaic current through the dispersion.

ACKNOWLEDGEMENTS

The support of the Office of Naval Research and the provision of precious metals by Johnson Matthey PLC is gratefully acknowledged.

REFERENCES

1. Z.G. Soos and P.J. Lingane, J. Phys. Chem. 68, 3821 (1964).

2. J.-L. Ponchon, K. Cespuglio, F. Gunon, M. Jouvet and J.-F. Pujol, Anal. Chem. 51, 1483 (1979).

3. M.A. Dayton, A.G. Ewing and R.M. Wightman, Anal. Chem. 52, 2392 (1980).

4. M. Kakihama, H. Ikeuchi, G.P. Sato and K. Tokuda, J. Electroanal. Chem. 108, 381 (1980).

5. R.M. Wightman, Anal. Chem. 53, 1125A (1981).

6. K.B. Oldham, J. Electroanal. Chem. 122, 1 (1981).

7. K. Aoki and J. Osteryoung, J. Electroanal. Chem. 122, 19 (1981).

8. J. Heinze, J. Electroanal. Chem. 124, 73 (1981).

9. K. Aoki and J. Osteryoung, J. Electroanal. Chem. 125, 315 (1981).

10. B. Scharifker and G.J. Hills, J. Electroanal. Chem. 130, 81 (1981).

11. D. Shoup and A. Szabo, J. Electroanal. Chem. 140, 237 (1982).

12. T. Hepel, W. Plot and J. Osteryoung, J. Phys. Chem. 87, 1278 (1983).

13. J.O. Howell and R.M. Wightman, Anal. Chem. 56, 524 (1984).

14. M. Fleischmann, F. Lasserre, J. Robinson and D. Swan, J. Electroanal. Chem. 177, 97 (1984).

15. M. Fleischmann, F. Lasserre and J. Robinson, J. Electroanal. Chem. 177, 115 (1984).

16. A.M. Bond, M. Fleischmann and J. Robinson, J. Electroanal. Chem. 180, 257 (1984).

17. A.M. Bond, M. Fleischmann and J. Robinson, J. Electroanal. Chem. 168, 299 (1984).

18. J. Cassidy, S.B. Khoo, S. Pons and M. Fleischmann, J. Phys. Chem. 89, 3933 (1985).

19. A.M. Bond, M. Fleischmann and J. Robinson, Extended Abstract, 165th Meeting of the Electrochemical Society, p. 523, May (1984). A.M. Bond, M. Fleischmann, S.B. Khoo, S. Pons and J. Robinson, submitted for publication.

20. M. Fleischmann, S. Bandyopadhyay and S. Pons, J. Phys. Chem. 89, 5537 (1985).

21. P. Bindra, A.P. Brown, M. Fleischmann and D. Pletcher, J. Electroanal. Chem. 58, 31 (1975).

22. P. Bindra, A.P. Brown, M. Fleischmann and D. Pletcher, J. Electroanal. Chem. 58, 39 (1975).

23. A.M. Bond, M. Fleischmann and J. Robinson, J. Electroanal. Chem., in press.

24. A. M. Bond et. al. personal communication.

25. J. Ghoroghchian, F. Sarfarazi, T. Dibble, J. Cassidy, J.J. Smith, A. Russell, M. Fleischmann, and S. Pons, submitted for publication.

26. N. Seeszynski, J. Osteryoung and M. Carter, Anal. Chem. 56, 130 (1984).

27. D. Shoup and A. Szabo, J. Electroanal. Chem. 160, 19 (1984).

28. M. Fleischmann, J. Ghoroghchian, and S. Pons, J. Phys. Chem. 89, 5530 (1985).

29. (a) M. Fleischmann, F. Goodridge and C.J.H. King, Brit. Pat. Appl. 16765 (1974).
(b) F. Goodridge, C.J.H. King and A.B. Wright, Electrochim. Acta 22, 1087 (1977).

30. M. Spiro and P.L. Freund, J. Chem. Soc. Faraday Trans. I 79, 1649 (1983).

31. P.L. Freund and M. Spiro, J. Phys. Chem. 89, 1074 (1985).

32. J. Kiwi and M. Gratzel, J. Am. Chem. Soc. 101, 7214 (1979).

33. M. Gratzel, Faraday Disc. Chem. Soc. 70, 359 (1980).

34. P. Keller and A. Mooadpour, J. Am. Chem. Soc. 102, 7193 (1980).

35. D. Meisel, W.A. Mulac and M.S. Matheson, J. Phys. Chem. 85, 179 (1981).

36. O. Johansen, A. Launikouis, J.W. Loder, A. S-H. Mau, W.H.F. Sasse, J.D. Swift and D. Wells, Aust. J. Chem. 34, 981 (1981).

37. D.S. Miller, A.J. Bard, G. McLendon and J. Ferguson, J. Am. Chem. Soc. 103, 5336 (1981).

38. D.S. Miller and G. McLendon, J. Am. Chem. Soc. 103, 6791 (1981).

39. W.J. Albery, P.N. Bartlett and A.J. McMahon in "Photogeneration of Hydrogen", A. Harriman and M.A. West, Eds., Academic Press, London (1982).

40. M.S. Matheson, P.C. Lee, D. Meisel and E. Pelizzetti, J. Phys. Chem. 87, 394, (1983).

41. W.J. Albery, P.N. Bartlett and A.J. McMahon, J. Electroanal. Chem. 182, 7 (1985).

42. J. Ghoroghchian, S. Pons, and M. Fleischmann, to be published.

43. D.R.Rolison, R.J. Nowak, S. Pons, M. Fleischmann, and J. Ghoroghchian, to be published.

44. C. Wagner and W. Traud, Z. Elektrochem. 44, 391 (1938).

45. M. Spiro in "The Physical Chemistry of Solutions", D.V. Fenby and I.D. Watson, Eds., Massey University Press, New Zealand (1983).

46. M. Spiro and A.B. Ravno, J. Chem. Soc. (1965), 78.

47. M. Spiro, J. Chem. Soc. Faraday Trans. 75, 1507 (1979).

48. P.L. Freund and M. Spiro, J. Chem. Soc. Faraday Trans. I 79, 481 (1983).

49. P.L. Freund and M. Spiro, J. Chem. Soc. Faraday Trans. I 79, 491 (1983).

50. W. Haller and H.C. Duecker, Journal of Research, National Bureau of Standards, 64A, 527 (1960).

51. J. Ghoroghchian, S. Pons, and M. Fleischmann, to be published.

Glossary of Symbols

a	radius of a particle (cm)
C	concentration of a given species (moles cm^{-3})
D	diffusion coefficient of a given species (cm^2 s^{-1})
E	electrode potential (V)
F	Faraday's constant (coulombs $mole^{-1}$)
i	current density (Amp cm^{-2})
I	current (Amp)
k_m	mass transfer coefficient (cm s^{-1})
L	distance between the feeder electrodes (cm)
n	number of electrons transferred per molecule
N	number of particles per unit volume (number cm^{-3})
N	Avagadro's constant (number $mole^{-1}$)
O	oxidized species of a redox couple
R	reduced species of a redox couple
	the gas constant (Joules $mole^{-1}$)
T	temperature (°)
v	volume of particles added per unit volume of solvent or solution (cm^3 cm^{-3})
V	voltage (V)
α	transfer coefficient
γ	polarization parameter
η	overpotential (V)
θ	angular position (rad)
λ	angular position (rad)
ν	rotational frequency (s^{-1})

ρ resistivity (ohm cm)

ϕ potential (V)

Ψ polarization parameter

ω angular velocity (rad s^{-1})

Ω monolayer coverage (moles cm^{-2})

Subscripts

o	denoting the exchange current
1,2	pertaining to species 1 and 2
appl	pertaining to the applied voltage
c	cathodic
lim	pertaining to the diffusion controlled current
N	pertaining to the net cross-sectional current density through the dispersion for one redox couple
r	pertaining to the reversible potential
R	pertaining to the current due to rotation of the particles
s	pertaining to the solution
T	pertaining to the cross-sectional current density
P	pertaining to the cross-sectional Faradaic current density through the dispersion

Superscript

m	pertaining to the mixture potential

Legends for figures

Figure 1A A representative particle and the coordinate system for single redox couple for $\alpha < 0.5$.

Figure 1B A representative particle and the distribution of cathodic and anodic reactions for two redox reactions.

Figure 2A The effect of α on the predicted normalized polarization curve for the dispersion for a single redox couple.

Figure 2B The effect of the difference in redox potential between two redox couples on the predicted normalized polarization plots for dispersion electrolysis and for $i_{o1}=i_{o2}$, $\alpha_1=\alpha_2=0.5$ and for the values $\Delta EF/4RT$ indicated.

Figure 2C The effect of the difference in redox potential and of the applied field between two redox couples (expressed as γ) on the predicted net normalized current density $I_N/3i_oV$ for one of the couples and on the ratio I_N/I_P for $i_{o1}=i_{o2}$. $\alpha_1=\alpha_2=0.5$ and for the values $\Delta EF/4RT$ indicated.

Figure 3A The cylindrical cell. The inner cylinder diameter was 2.2 cm and the outer cylinder diameter was 3.2cm. The platinum electrode cylinder height was 5.5cm.

Figure 3B The plane parallel capillary gap cell and the electrolysis system. The electrodes are 2.5cm square, and the gap thickness is 0.5mm.

Figure 4 Polarization curves for hydrogen evolution/oxidation in conductivity water at low values of the applied field. 6.3×10^8 Pt particles cm^{-3}, diameter 2.5m. ◇ background current, + 10% H_2 + 90% N_2; □ 100% H_2 total pressure 1 atm.

Figure 5 Comparison of experimental polarization plots for hydrogen evolution/oxidation with the predicted forms of these plots (full lines for $\alpha=0.5$, $\alpha=0.25$ or 0.75, $\alpha=0$ or 1) 6.3×10^9 Pt particles cm^{-3}, diameter 2.5μ

A low values of γ; apparent exchange current density 120mA cm^{-2}

B low values of ψ; apparent exchange current density 55mA cm^{-2}

C high values of γ; apparent exchange current density 50mA cm^{-2}

D high values of ψ; apparent exchange current density 22mA cm^{-2}

Figure 6 Polarization plots for oxygen evolution/reduction in 10^{-4} M KOH. Diameter of Pt particles 2.5μ.

6.3×10^8 particles cm^{-3}

3.6×10^8 particles cm^{-3}

1.8×10^8 particles cm^{-3}

Figure 7 Polarization curves for oxygen evolution/reduction in 10^{-6} M KOH. Diameter of Pt particles 2.5μ.

1.8×10^8 particles cm^{-3}

3.6×10^8 particles cm^{-3}

Figure 1a

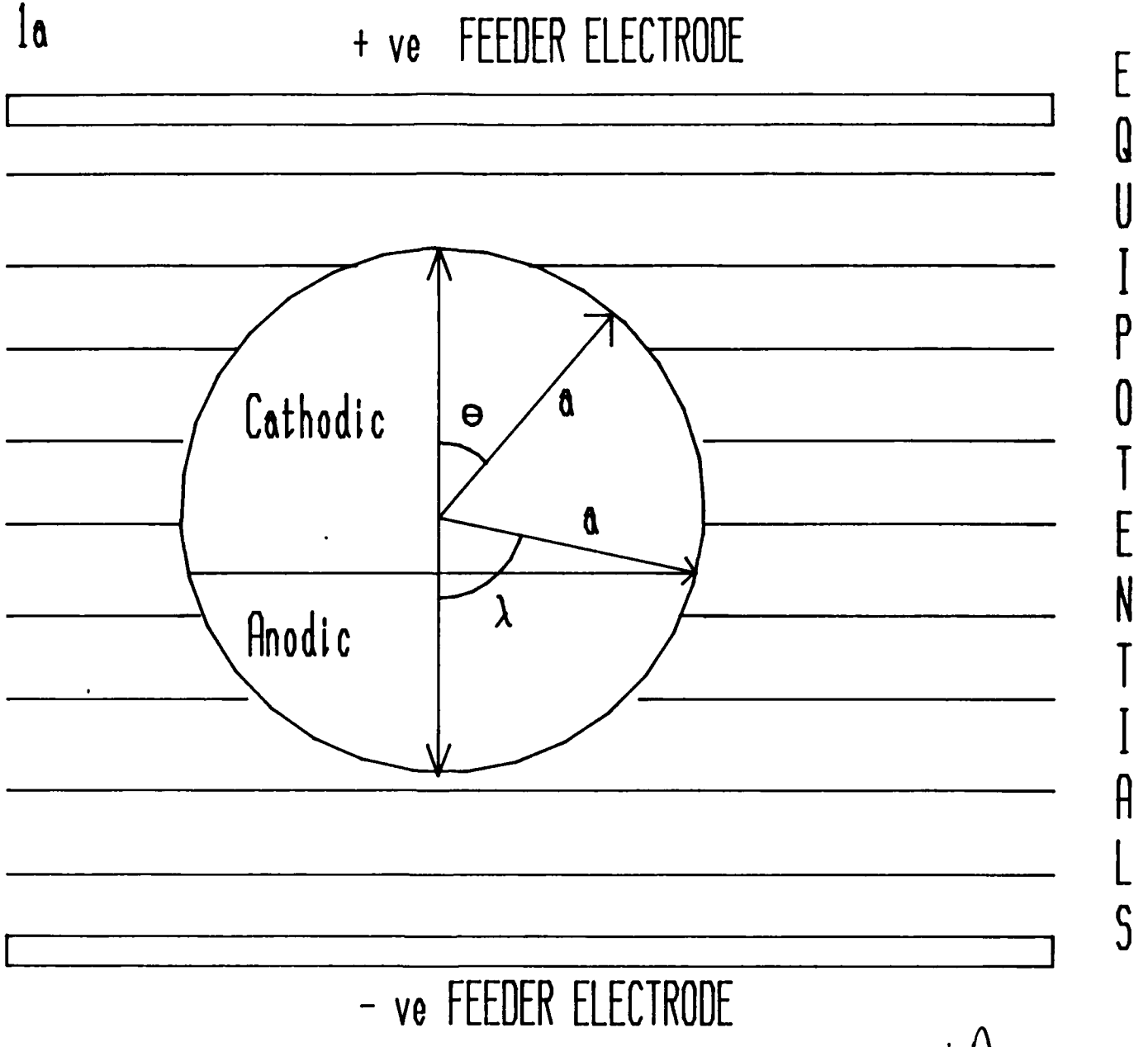
+ ve FEEDER ELECTRODE
Cathodic
Anodic
θ
a
a
λ
EQUIPOTENTIALS
- ve FEEDER ELECTRODE
iA

Figure 1b

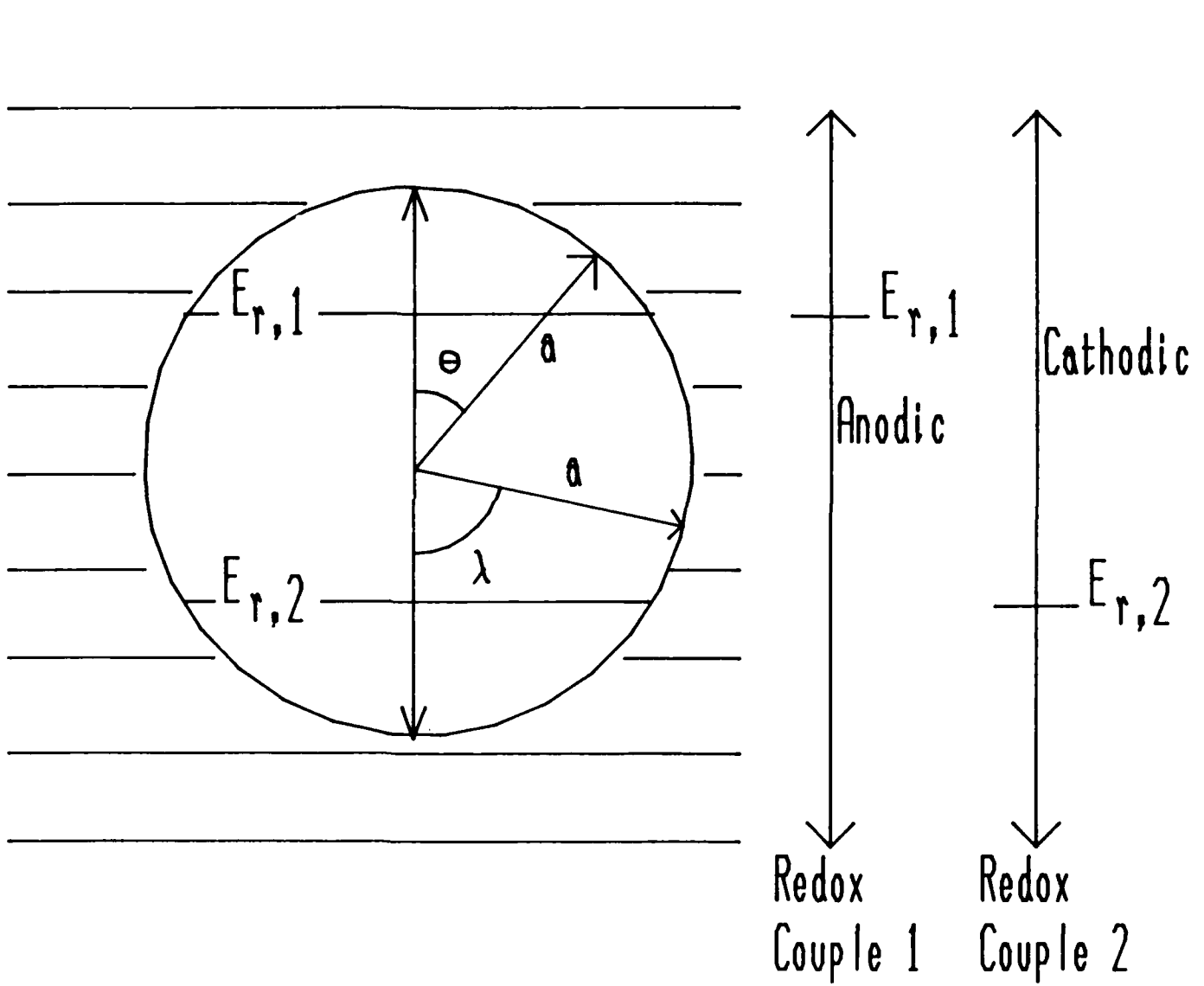
EQUIPOTENTIALS
$E_{r,1}$
$E_{r,2}$
θ
a
a
λ
$E_{r,1}$
Anodic
Cathodic
$E_{r,2}$
Redox Couple 1
Redox Couple 2

PREDICTED POLARIZATION PLOTS

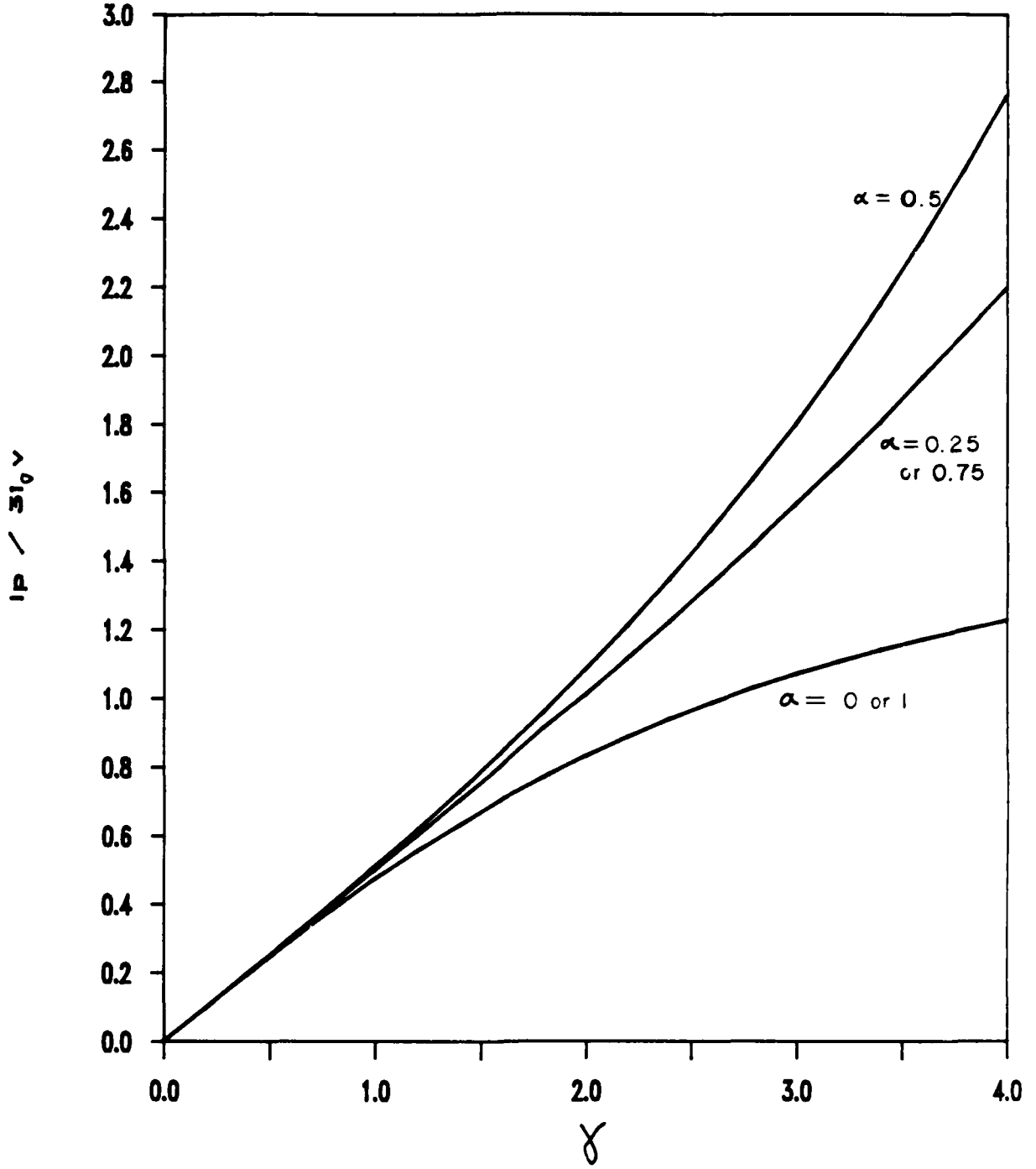

ZA

PREDICTED POLARIZATION PLOTS

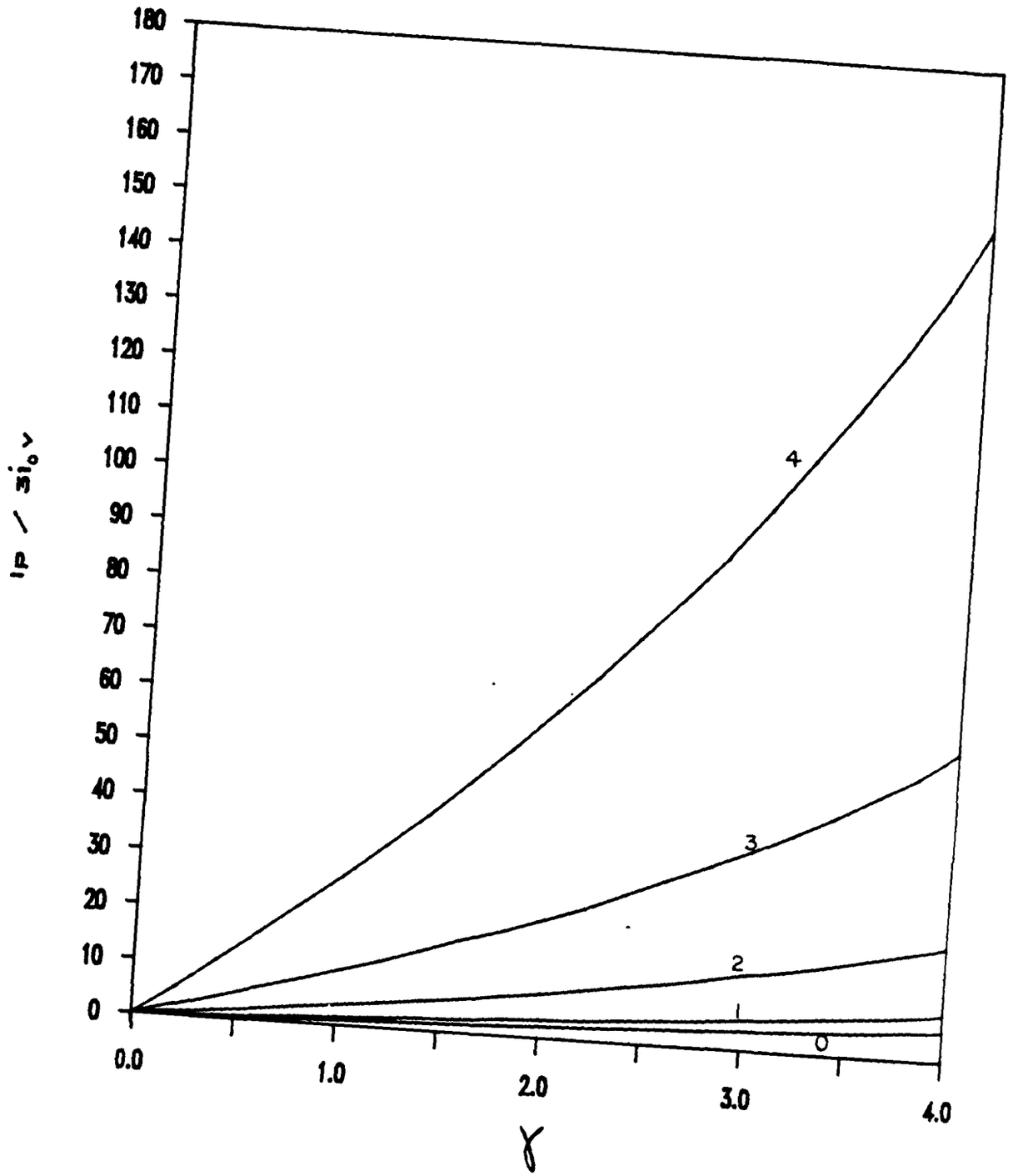

ZB

NET RATE OF EACH REDOX REACTION

AND THE RATIO Ip / In

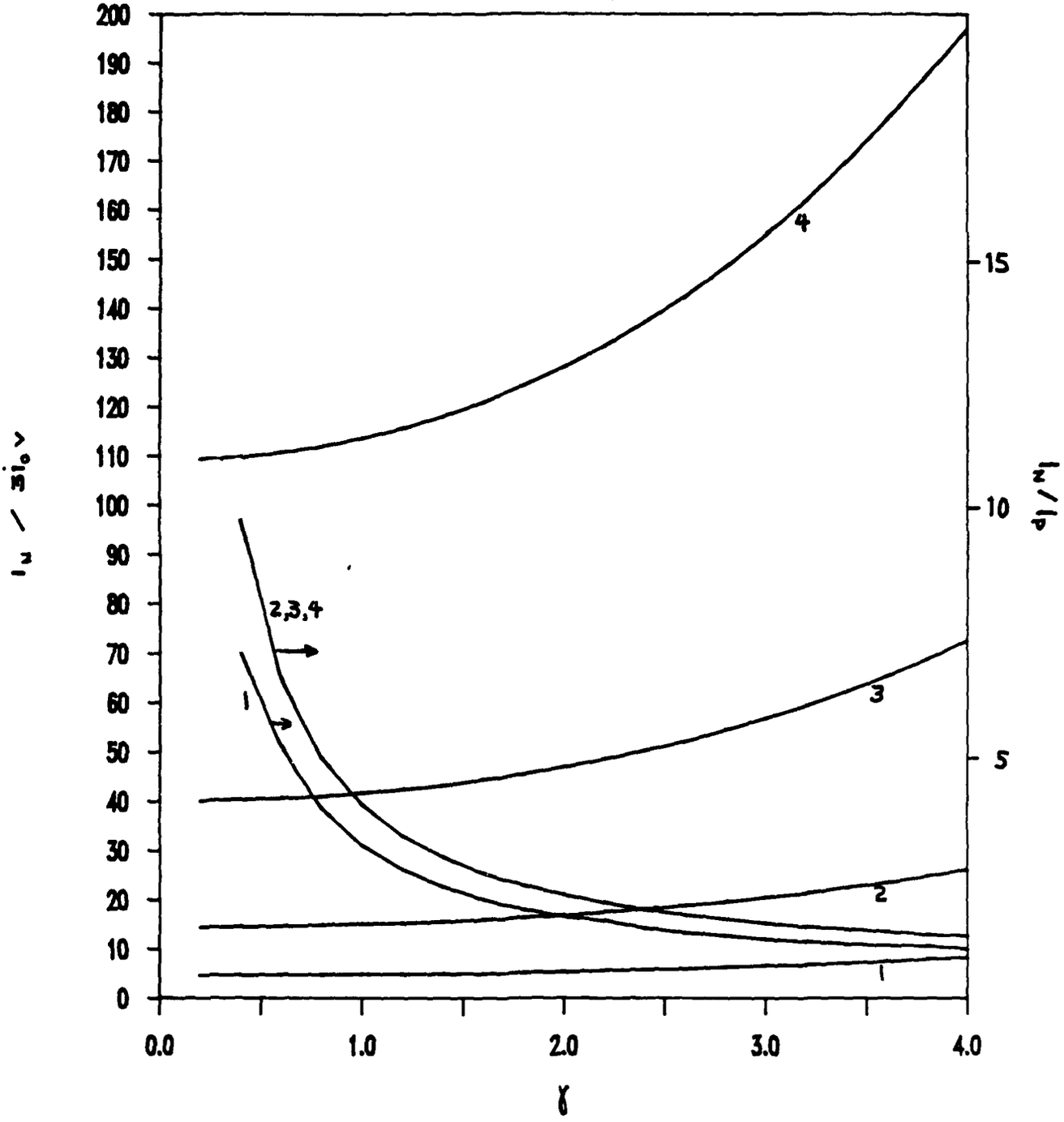

2C

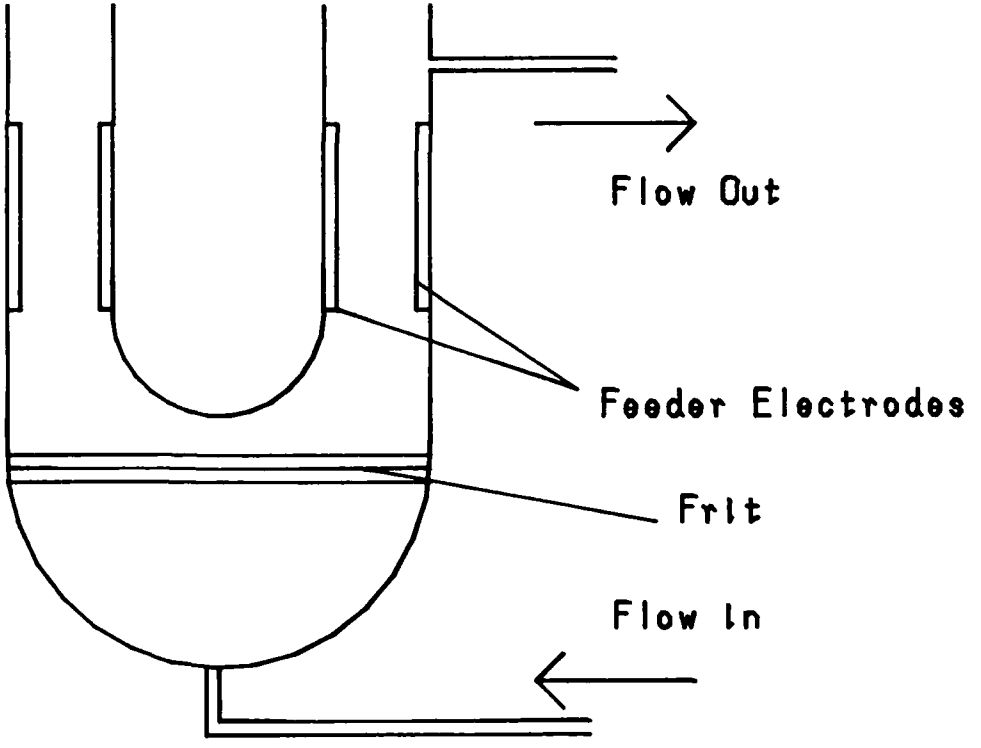

3A

Cell Detail

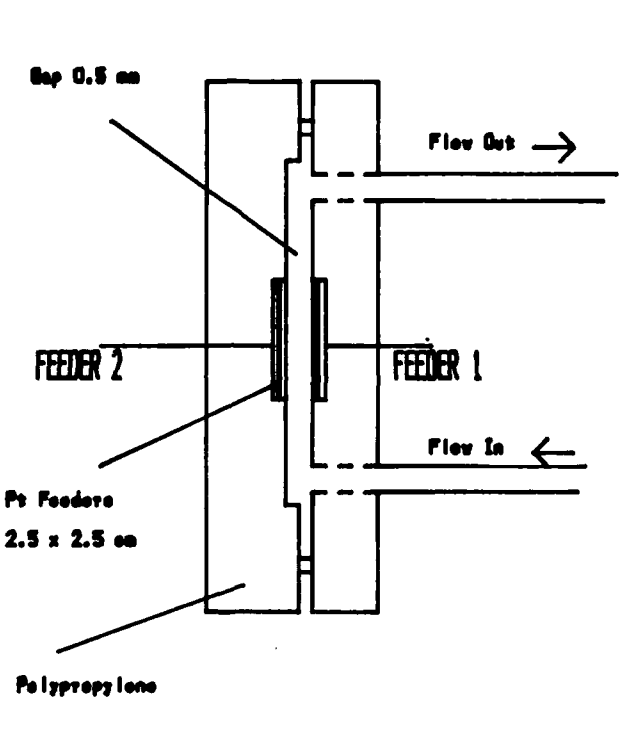

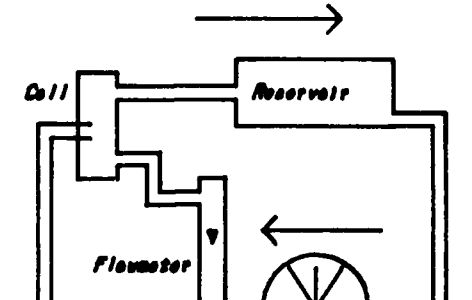

Dispersion Electrolysis System

3B

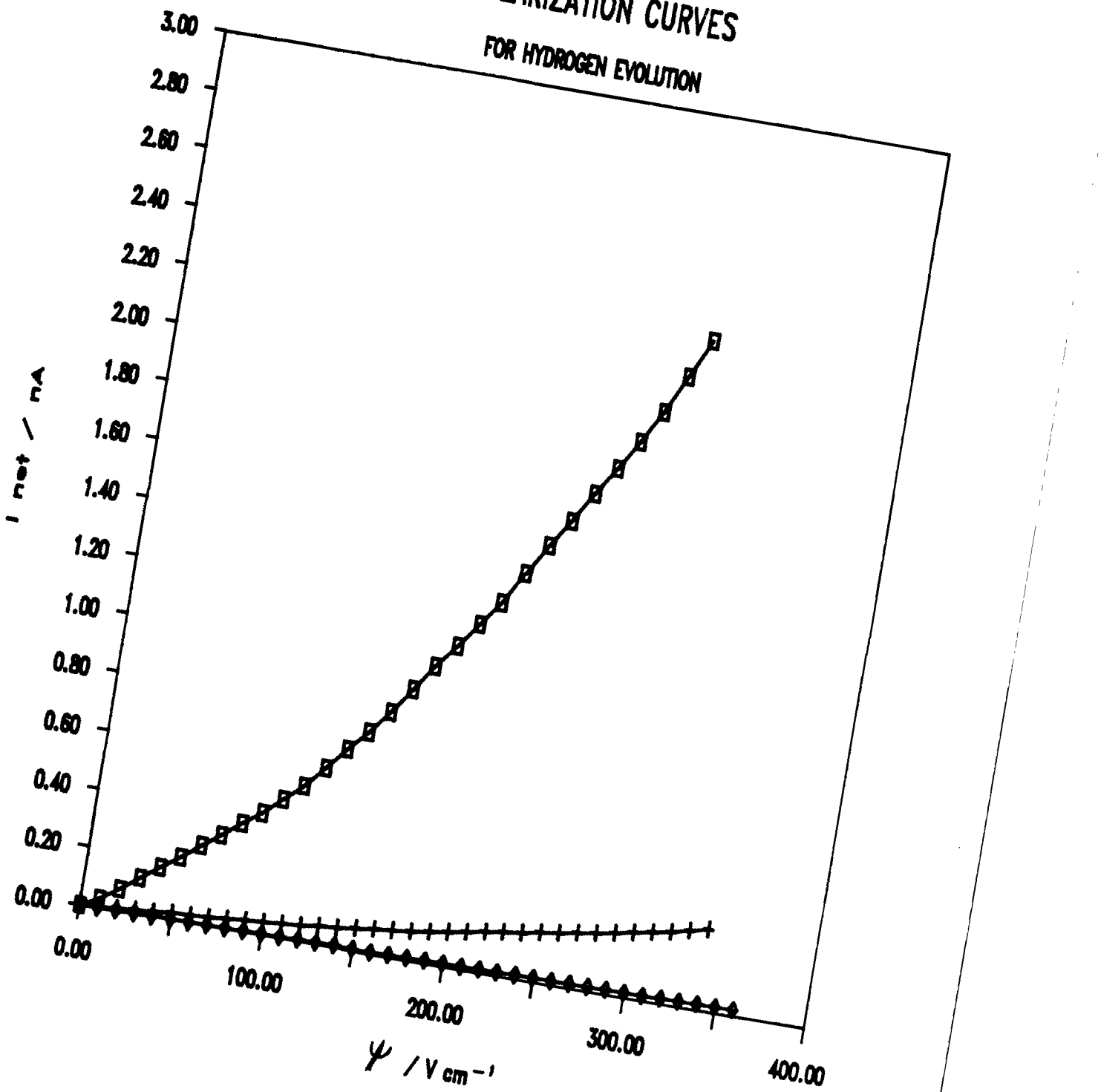
POLARIZATION CURVES
FOR HYDROGEN EVOLUTION
3.00
2.80
2.60
2.40
2.20
2.00
1.80
1.60
1.40
1.20
1.00
0.80
0.60
0.40
0.20
0.00
0.00
100.00
200.00
300.00
400.00
ψ / V cm⁻¹

DIMENSIONLESS POLARIZATION PLOTS

FOR HYDROGEN EVOLUTION/ OXIDATION

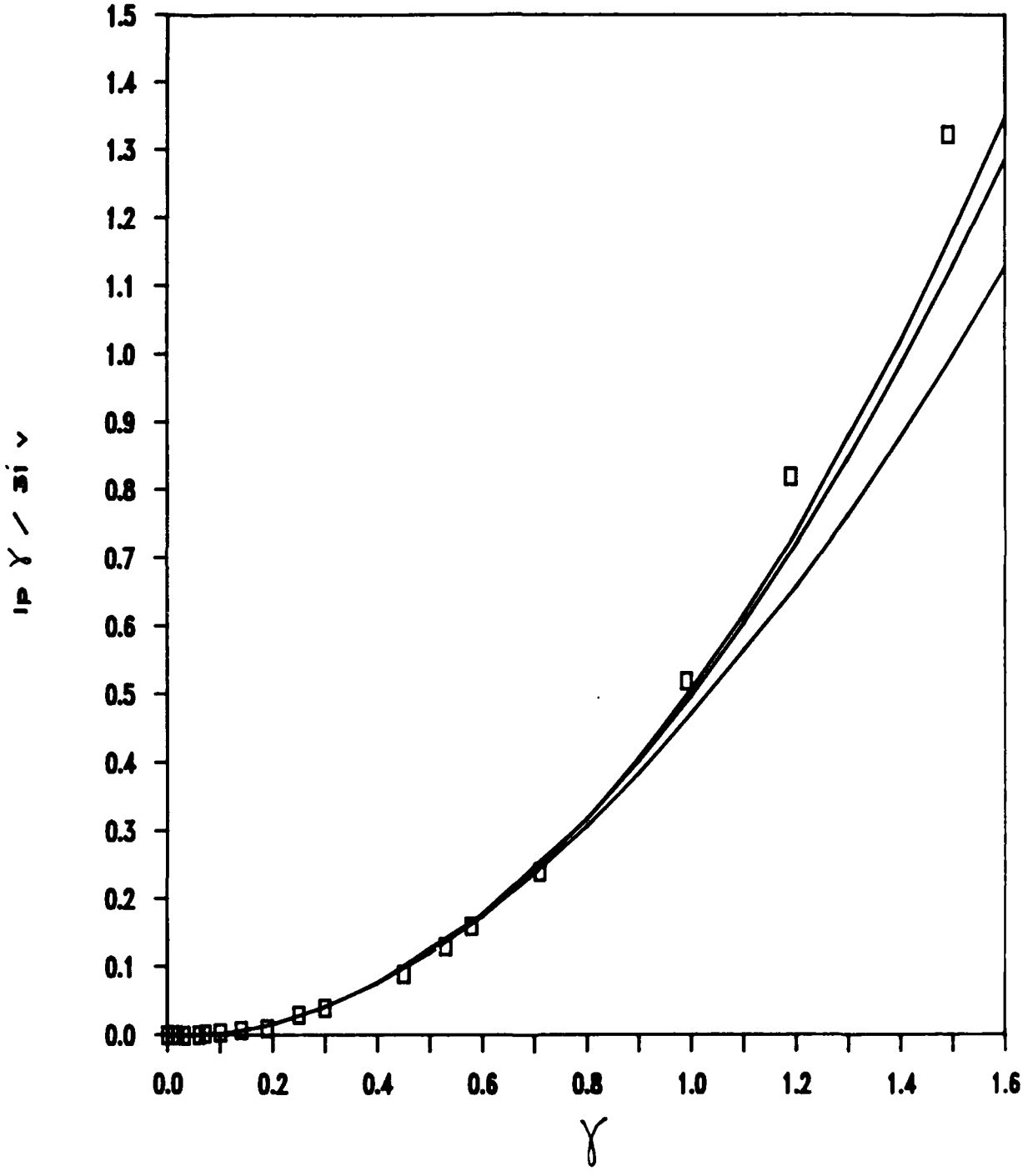

DIMENSIONLESS POLARIZATION PLOTS

FOR HYDROGEN EVOLUTION/ OXIDATION

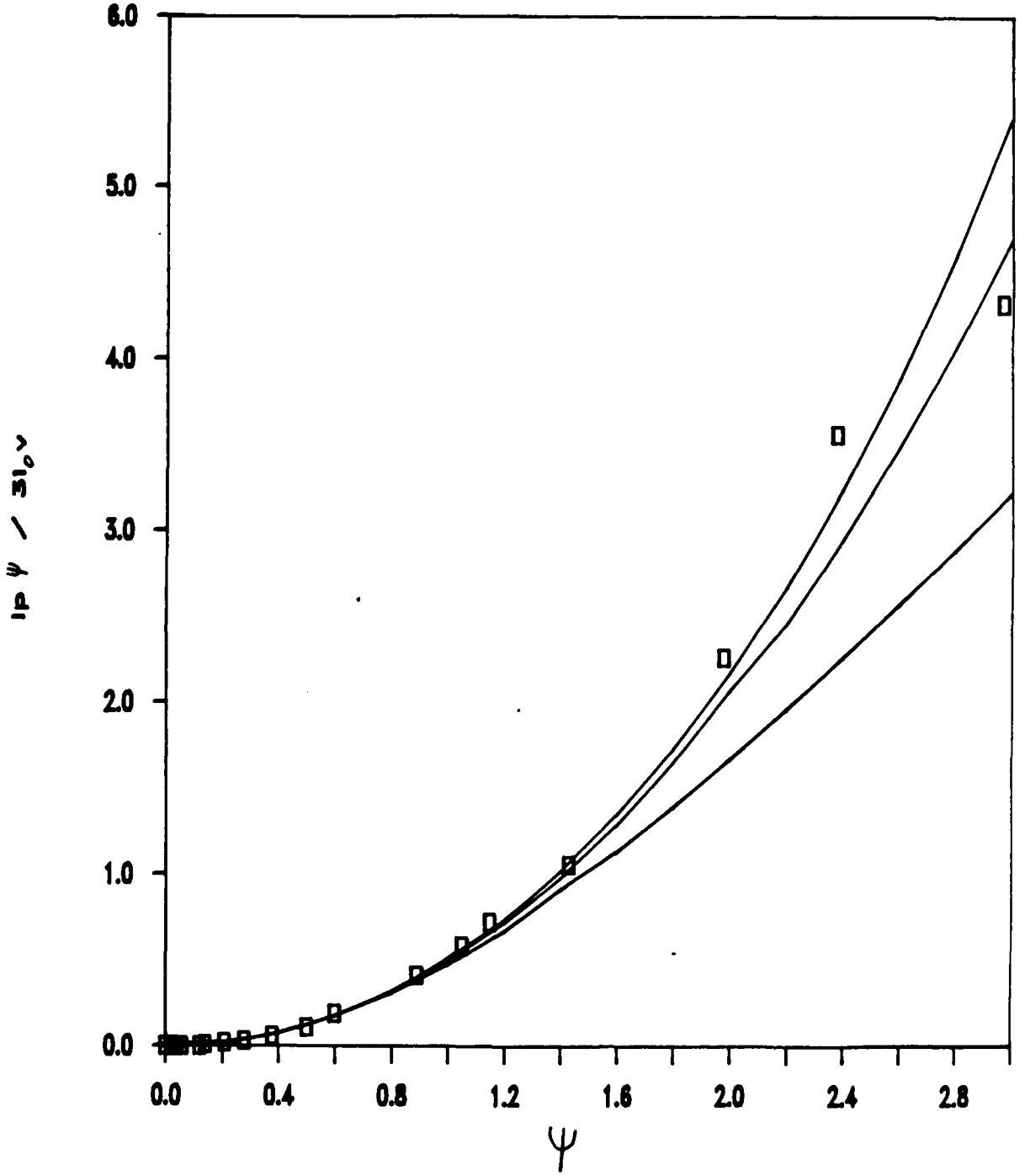

5B

DIMENSIONLESS POLARIZATION PLOTS

FOR HYDROGEN EVOLUTION/ OXIDATION

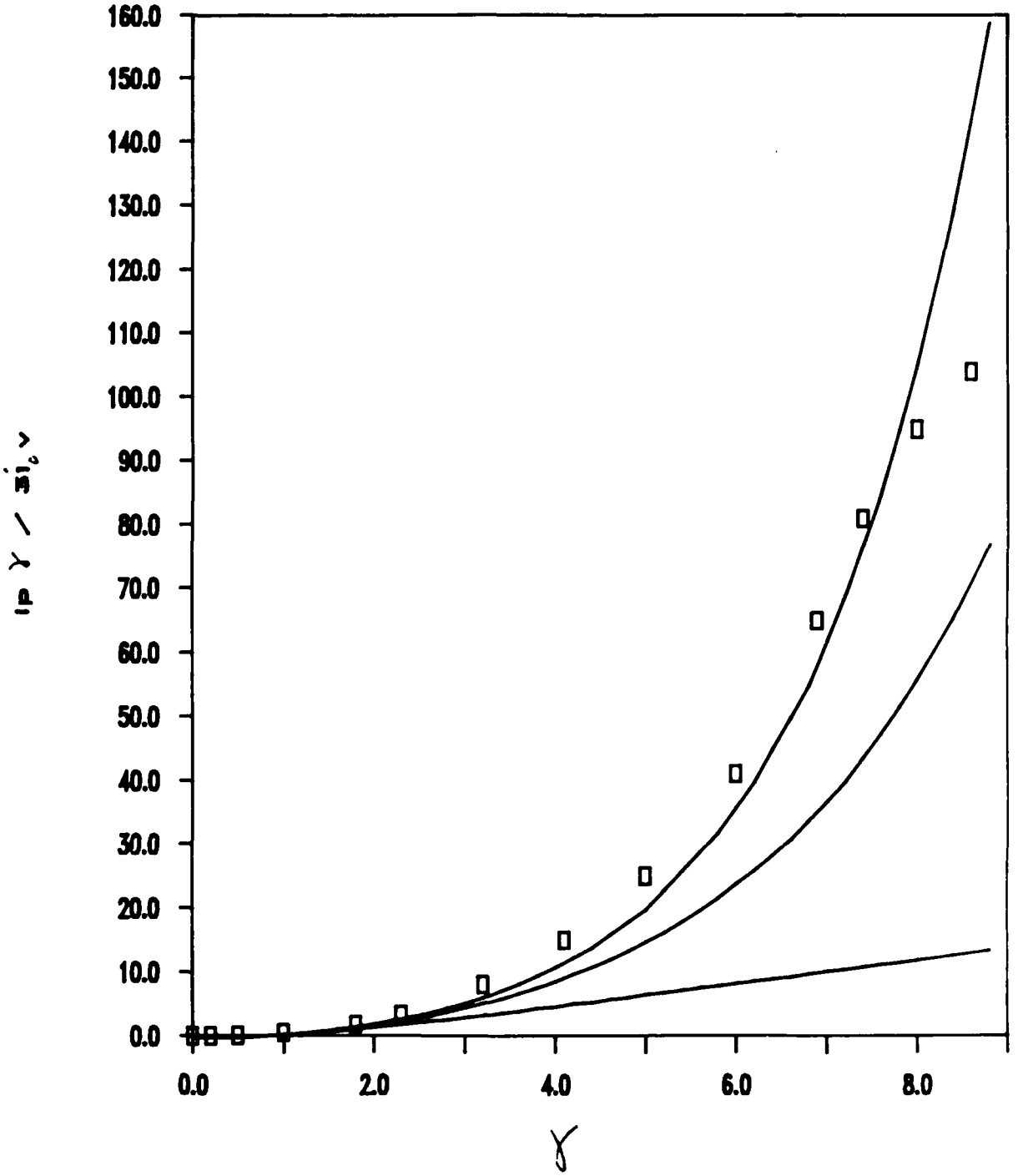

DIMENSIONLESS POLARIZATION PLOTS

FOR HYDROGEN EVOLUTION/ OXIDATION

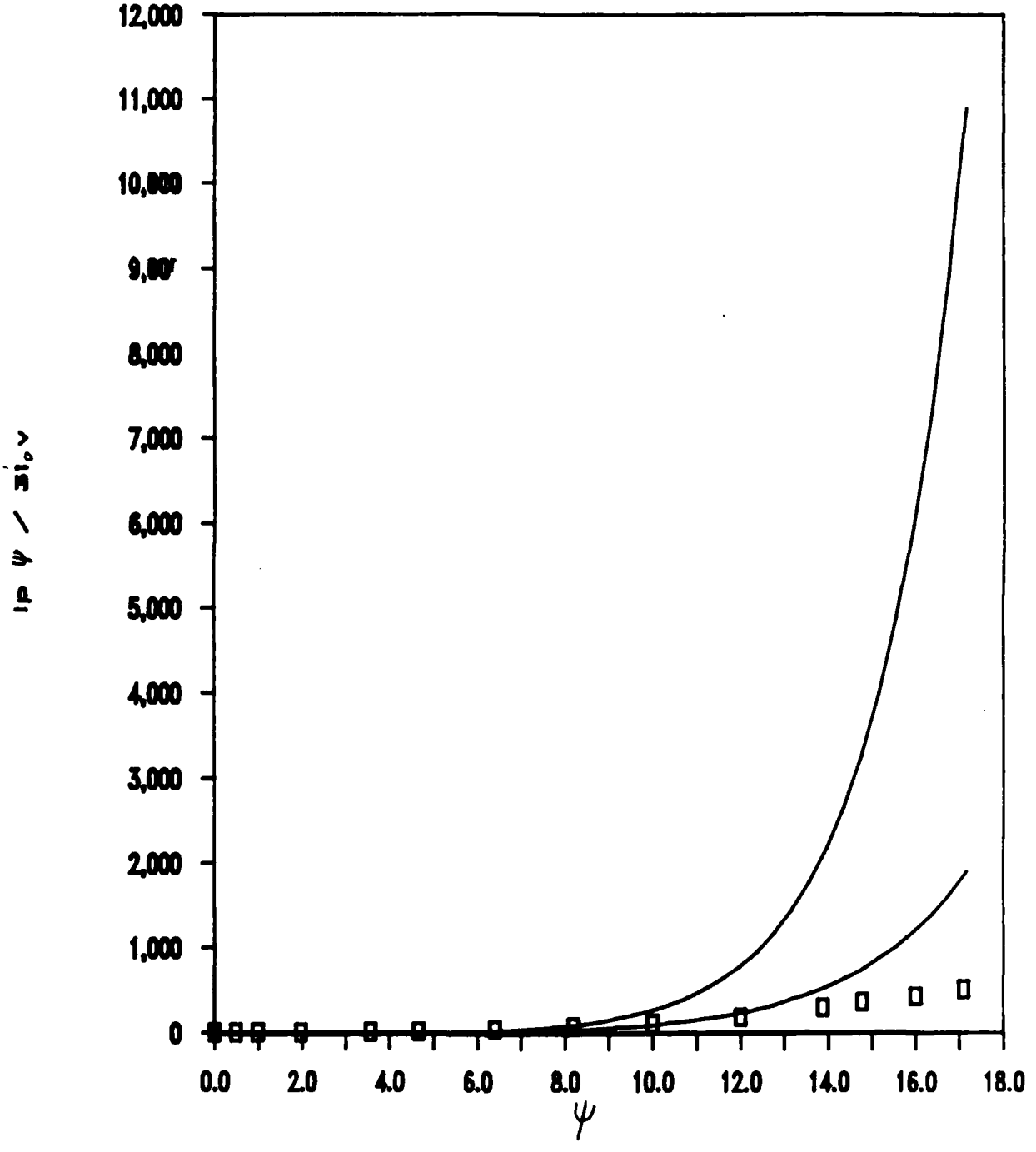

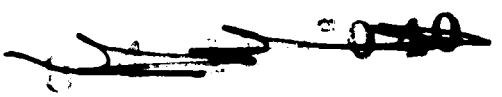

5D

POLARIZATION PLOT

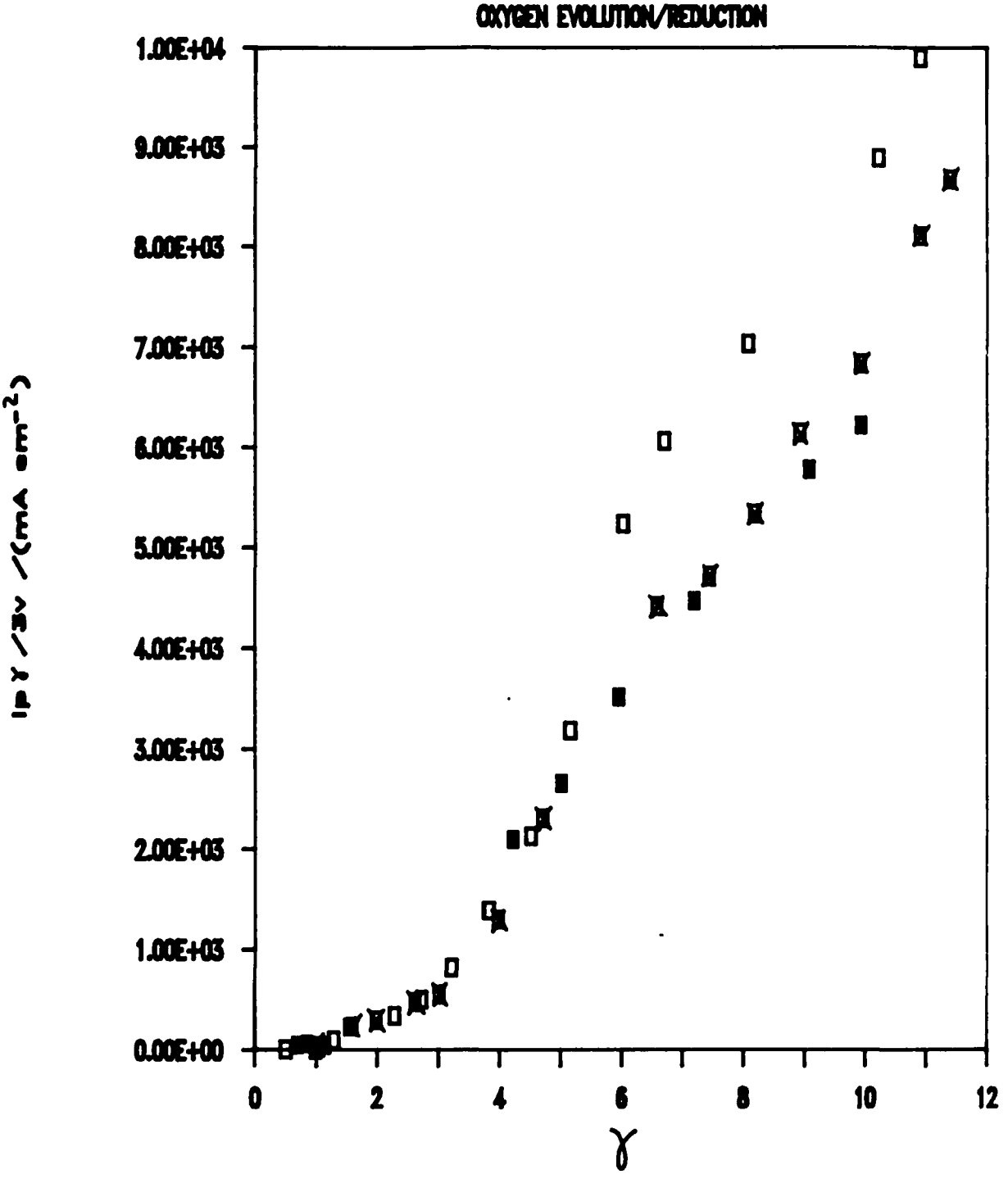

POLARIZATION CURVES

FOR OXYGEN EVOLUTION

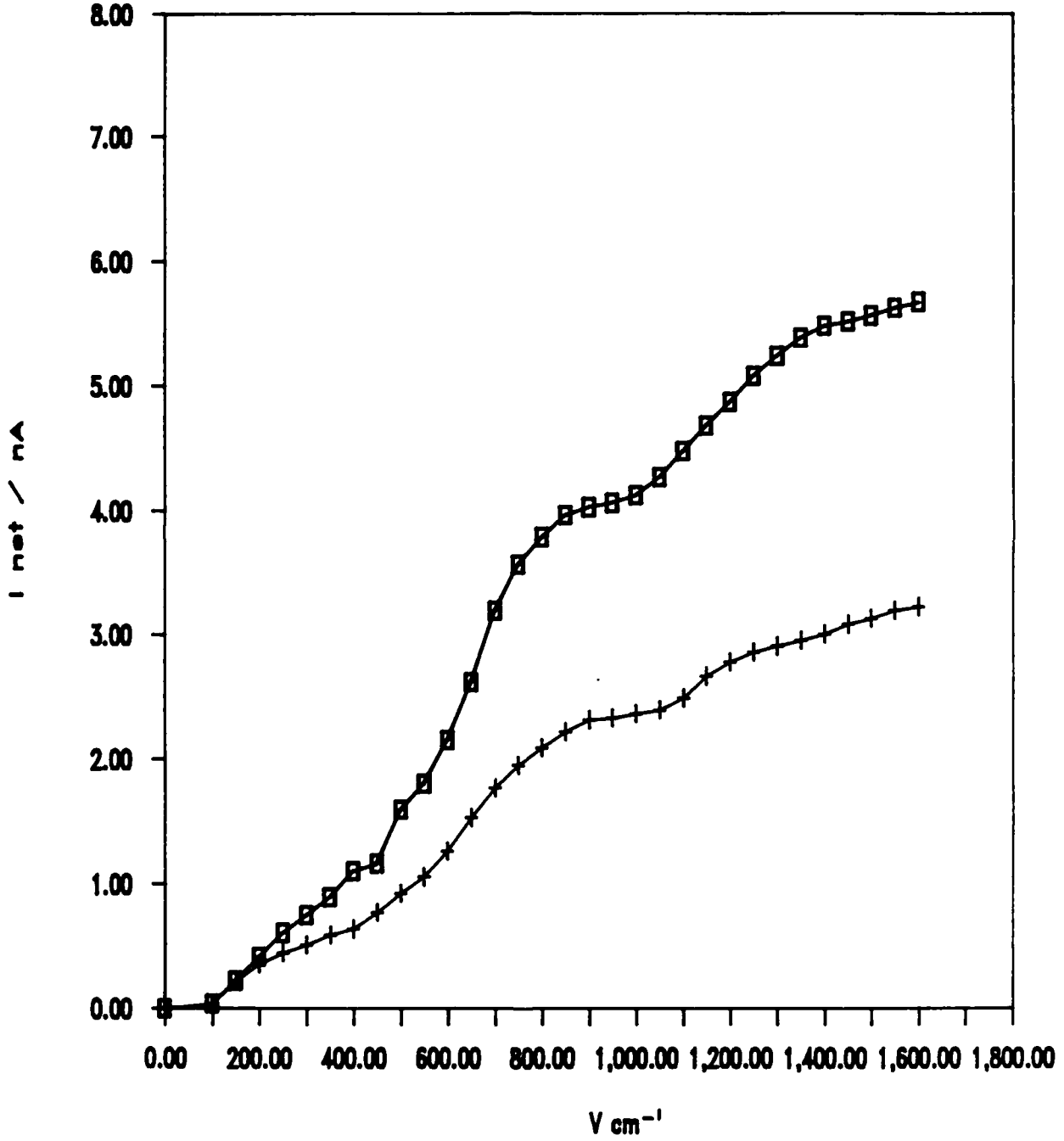

7

DL/413/83/01
GEN/413-2

TECHNICAL REPORT DISTRIBUTION LIST, GEN

	No. Copies
Office of Naval Research Attn: Code 413 800 N. Quincy Street Arlington, Virginia 22217	2
Dr. Bernard Douda Naval Weapons Support Center Code 5042 Crane, Indiana 47522	1
Commander, Naval Air Systems Command Attn: Code 310C (H. Rosenwasser) Washington, D.C. 20360	1
Naval Civil Engineering Laboratory Attn: Dr. R. W. Drisko Port Hueneme, California 93401	1
Defense Technical Information Center Building 5, Cameron Station Alexandria, Virginia 22314	12
DTNSRDC Attn: Dr. G. Bosmajian Applied Chemistry Division Annapolis, Maryland 21401	1
Dr. William Tolles Superintendent Chemistry Division, Code 6100 Naval Research Laboratory Washington, D.C. 20375	1
Dr. David Young Code 334 NORDA NSTL, Mississippi 39529	1
Naval Weapons Center Attn: Dr. Ron Atkins Chemistry Division China Lake, California 93555	1
Scientific Advisor Commandant of the Marine Corps Code RD-1 Washington, D.C. 20380	1
U.S. Army Research Office Attn: CRD-AA-IP P.O. Box 12211 Research Triangle Park, NC 27709	1
Mr. John Boyle Materials Branch Naval Ship Engineering Center Philadelphia, Pennsylvania 19112	1
Naval Ocean Systems Center Attn: Dr. S. Yamamoto Marine Sciences Division San Diego, California 91232	1

DL/413/83/01
359/413-2

ABSTRACTS DISTRIBUTION LIST, 359/627

Dr. M. Wrighton
Chemistry Department
Massachusetts Institute
of Technology
Cambridge, Massachusetts 02139

Dr. B. Stanley Pons
Department of Chemistry
University of Utah
Salt Lake City, Utah 84112

Donald E. Mains
Naval Weapons Support Center
Electrochemical Power Sources Division
Crane, Indiana 47522

S. Ruby
DOE (STOR)
Room 5E036 Forrestal Bldg., CE-14
Washington, D.C. 20595

Dr. A. J. Bard
Department of Chemistry
University of Texas
Austin, Texas 78712

Dr. Janet Osteryoung
Department of Chemistry
State University of New York
Buffalo, New York 14214

Dr. Donald W. Ernst
Naval Surface Weapons Center
Code R-33
White Oak Laboratory
Silver Spring, Maryland 20910

Mr. James R. Moden
Naval Underwater Systems Center
Code 3632
Newport, Rhode Island 02840

Dr. Bernard Spielvogel
U.S. Army Research Office
P.O. Box 12211
Research Triangle Park, NC 27709

Dr. Aaron Fletcher
Naval Weapons Center
Code 3852
China Lake, California 93555

Dr. M. M. Nicholson
Electronics Research Center
Rockwell International
3370 Miraloma Avenue
Anaheim, California

Dr. Michael J. Weaver
Department of Chemistry
Purdue University
West Lafayette, Indiana 47907

Dr. R. David Rauh
EIC Laboratories, Inc.
111 Downey Street
Norwood, Massachusetts 02062

Dr. Aaron Wold
Department of Chemistry
Brown University
Providence, Rhode Island 02192

Dr. Martin Fleischmann
Department of Chemistry
University of Southampton
Southampton SO9 5NH ENGLAND

Dr. R. A. Osteryoung
Department of Chemistry
State University of New York
Buffalo, New York 14214

Dr. John Wilkes
Air Force Office of Scientific
Research
Bolling AFB
Washington, D.C. 20332

Dr. R. Nowak
Naval Research Laboratory
Code 6171
Washington, D.C. 20375

Dr. D. F. Shriver
Department of Chemistry
Northwestern University
Evanston, Illinois 60201

DL/413/83/01
359/413-2

ABSTRACTS DISTRIBUTION LIST, 359/627

Dr. Robert Somoano
Jet Propulsion Laboratory
California Institute of Technology
Pasadena, California 91103

Dr. Johann A. Joebstl
USA Mobility Equipment R&D Command
DRDME-EC
Fort Belvoir, Virginia 22060

Dr. Judith H. Ambrus
NASA Headquarters
M.S. RTS-6
Washington, D.C. 20546

Dr. Albert R. Landgrebe
U.S. Department of Energy
M.S. 6B025 Forrestal Building
Washington, D.C. 20595

Dr. J. J. Brophy
Department of Physics
University of Utah
Salt Lake City, Utah 84112

Dr. Charles Martin
Department of Chemistry
Texas A&M University
College Station, Texas 77843

Dr. H. Tachikawa
Department of Chemistry
Jackson State University
Jackson, Mississippi 39217

Dr. Theodore Beck
Electrochemical Technology Corp.
3935 Leary Way N.W.
Seattle, Washington 98107

Dr. Farrell Lytle
Boeing Engineering and
Construction Engineers
P.O. Box 3707
Seattle, Washington 98124

Dr. Robert Gotscholl
U.S. Department of Energy
MS G-226
Washington, D.C. 20545

Dr. Edward Fletcher
Department of Mechanical Engineering
University of Minnesota
Minneapolis, Minnesota 55455

Dr. John Fontanella
Department of Physics
U.S. Naval Academy
Annapolis, Maryland 21402

Dr. Martha Greenblatt
Department of Chemistry
Rutgers University
New Brunswick, New Jersey 08903

Dr. John Wasson
Syntheco, Inc.
Rte 6 - Industrial Pike Road
Gastonia, North Carolina 28052

Dr. Walter Roth
Department of Physics
State University of New York
Albany, New York 12222

Dr. Anthony Sammells
Eltron Research Inc.
4260 Westbrook Drive, Suite 111
Aurora, Illinois 60505

Dr. C. A. Angell
Department of Chemistry
Purdue University
West Lafayette, Indiana 47907

Dr. Thomas Davis
Polymer Science and Standards
Division
National Bureau of Standards
Washington, D.C. 20234

Ms. Wendy Parkhurst
Naval Surface Weapons Center R-33
R-33
Silver Spring, Maryland 20910

END

DATE

FILMED

6-1988

DTIC